DEVELOPMENT OF A NEW COMPUTER MODEL FOR THE SIMULATION OF COOKING ORGANIC AEROSOL FORMATION FROM HEATED COOKING OILS USING ASPEN PLUS

Fariza Aldemkhan, Bachelor in Chemical Engineering

Submitted in fulfillment of the requirements for the degree of Master of Science in Chemical Engineering

School of Engineering

Department of Chemical Engineering

Nazarbayev University

53 KABANBAY BATYR AVENUE,

ASTANA, KAZAKHSTAN, 010000

Supervisors: Mehdi Amouei Torkmahalleh & Dhawal Shah

May 2018

DECLARATION

I hereby, declare that this manuscript, entitled “Development of a new computer model for the simulation of cooking organic aerosol formation from heated vegetable oils using Aspen Plus”, is the result of my own work except for quotations and citations which have been duly acknowledged. I also declare that, to the best of my knowledge and belief, it has not been previously or concurrently submitted, in whole or in part, for any other degree or diploma at Nazarbayev University or any other national or international institution.

_____

Name: Fariza Aldemkhan

Date: May 4, 2018

Abstract

Cooking is an important source of particulate matter with adverse effects on human health, particularly in developing countries where simple stoves burning biomass (wood, animal dung, and crop waste) and coal are used [1]. Depending on the components of the food, the composition of cooking organic aerosol (COA) may vary drastically. However, due to loss of volatile organic compounds (VOC) during experiments and numbers of other uncertainties, the exact compositions and rates of COA formation are difficult to be determined. In this thesis, a simulation model for heating corn, soybean and sunflower oils and stir-frying myrcia was developed using Aspen Plus.

Frying is a highly dynamic process, where radical chain reactions take place. However, in this model, thermodynamic equilibrium was assumed. In order to reproduce frying process, two reactors simulating the chemical alterations taking place in oils while frying were employed. One simulates hydrolysis reactions, where triglycerides decompose into mono-, diglycerides, free fatty acids, and glycerol, whilst another simulates oxidation and thermal alteration reactions that occur simultaneously. These reactors were included as the heating temperature exceeded the smoke point of cooking oils. Output streams from these reactors were mixed with air and cooled to mimic rapid dilution. Lastly, nucleation process responsible for particle formation was shown in flash separators.

The simulation results showed that heating corn oil at 240 °C produced non-polar triglyceride dimers, oxidized triglyceride monomers with one of the free fatty acids oxidized by keto-, epoxy, or hydroxy- groups and triglycerides with cyclic fatty acids. Moreover, two types of oxidized triglyceride dimers were observed: two unaltered triglycerides joined by oxygen, and oxidized dimer with one monomer oxidized. Additionally, the volatile organic compounds (VOCs) emitted from heated oils were dominated by light aldehydes (ethanal, butanal, and propanal), alkanes (pentane) and cycloalkenes (cycloheptadiene) consistent with experimental results [2]. The primary organic aerosol (POA) emission rates from heating soybean and sunflower oils were higher than that from corn oil, due to higher compositions of unsaturated fatty acids, and thus, lower smoke point. Stir-frying myrcia in corn oil increased POA emission rate by 1.5 as the contribution of organic compounds to particulate matter (PM) increased. In addition to VOCs emitted from heated corn oil, stir-frying myrcia generated terpenes, terpenoids, aldehydes (octanal, nonanal) and methylpyrrole consistent with its composition. Increasing the temperature of oil increased the particulate matter formation rate, whereas increasing the indoor temperature had an opposite effect. It was found that nucleation of VOCs to form PM starts at the height above the pan where the temperature of vapors is equivalent to 36°C.

Acknowledgements

First of all, I would like to extend my sincerest thanks and appreciation to supervisor Mehdi Amouei Torkmahalleh for helping me accomplish this thesis and sharing his professional expertise. I appreciate the contribution of external supervisor Philip Hopke and co-supervisor Dhawal Shah for their time and consideration.

I would like to thank Nazarbayev University and especially all of School of Engineering staff for the opportunity to persuade Masters Degree and achieve my professional and academic goals.

Finally, I would like to extend eternal gratitude to my family and friends for supporting me. I would like to thank my husband for supporting my endeavors.

Table of Contents

List of Figures

List of Tables

Chapter 1- Introduction

Airborne particulate matters, consisting of liquid or solid particles suspended in air, play a key role in many atmospheric processes. A significant fraction of particulate matter (PM) corresponds to organic aerosols (OA) that have adverse effects on the air quality and, thus, human health [3]. The organic aerosol is known to be originated from a variety of different sources [4]. Among which, particulate organic matter from cooking operations constitutes to 18-20% of OA [5]. Therefore, cooking activity indoors is considered as one of the most significant contributors to OA, and organic particles produced as a result of cooking are referred to as cooking organic aerosol (COA) [6].

The rate of COA formation and nature of emitted chemical species depend on the variety of factors. The factors include a method of cooking such as charbroiling [7], deep-frying, stir-frying, baking, grilling, boiling [6] and source of heat like oven, electric and gas stoves [8]. Moreover, the use of different ingredients including various vegetable oils [9], additives [10], [11] and the food being cooked [6] have an individual footprint on the indoor chemistry. Each food component contributes to the production of a highly complex mixture of many tens of thousands of species that potentially have a substantial effect on human health [4].

The determination of the impact of the COA on the health and climate has significant uncertainties, as there is a lack of knowledge on their sources,

composition, properties, and mechanism of formation [12]. The primary mechanism of COA formation is thought to be the nucleation of the supersaturated volatile organic compounds (VOCs) produced during cooking operations [13]. That is, COA is mainly composed of primary organic aerosol (POA) which is directly emitted to the atmosphere.

The POA is anticipated to be mainly composed of fine and ultrafine particles. That is, the particles with the diameter less than 2.5 μm and 100 nm, respectively [4]. These particles are small enough to penetrate deeper into the respiratory system than more coarse PM_{10} and, as a result of long-term exposure, heart and lung diseases leading to death can develop [14].

In addition to particle size, the composition of POA also plays role in its effect on health. The composition of the POAs produced from cooking depends on the chemical and physical processes that occur within the source [15]. The moisture, air and high temperature are three major causative agents that initiate the reactions occurring in oil while frying food; these are: hydrolysis, oxidation, and thermal alteration, respectively [16], [17]. Edible oils and fats consist primarily of triglycerides [18]. As a result of liquid phase reactions altering the triglyceride, organic compounds such as free fatty acids, monomers and dimers of oxidized triglycerides, and cyclic triglycerides are produced. Moreover, VOCs from the decomposition of the free fatty acids contain aldehydes, alkanes, alcohols and ketones that condensate to form COA [19]. Therefore, in the given context of cooking, COA and POA were used interchangeably.

Due to rapid evaporation of VOC emitted during frying, determination of the POA's composition, physical parameters and rate of formation includes uncertainties [13]. Moreover, the dependence of POA on the specific causative agent mentioned above is difficult to determine due to the errors related to experiments. These uncertainties could be minimized by employing the computer simulations. The simulation can consider the chemical and physical changes occurring in the oil being used. One of the recent works in this direction was simulating the heating of various vegetable oils including olive, peanut, safflower, soybean, canola, corn and coconut oils below their smoke points in Aspen Plus [13]. Smoke point is the temperature at which visible smoke appears above the pan. Amouei Torkmahalleh assumed that there are no chemical reactions taking place below the smoke point. In this simulation, it was found that rate of PM formation depends on indoor air temperature, heating temperature, the composition of the oil and additives.

Aspen Plus is a chemical engineering software developed by Aspen Tech Inc. that allows simulating the process by applying the mass and energy balances on the system, and methods predicting phase and chemical equilibrium. It comprises a wide range of chemical components and their physical properties, unit operations and thermodynamic models that are chosen to mimic the real chemical and physical processes. Compared to experiments, the simulation in Aspen Plus has an advantage of a better control of the independent variables. That is, the effect of various factors on the COA formation can be investigated.

Heating three individual cooking oils including corn, soybean, and sunflower oils were simulated using Aspen Plus. The temperature of the oils was set as at 240 °C which is higher than smoke point of these oils. The aim of this simulation is to set up a model incorporating major chemical reactions in the liquid phase and showing the contribution of VOCs to COA that helps determine its physical properties at given operating conditions. The emissions are further processed to observe the sources of the COA and estimate the contribution of both oil and herb components. Moreover, the response of the simulation to change of parameters such as indoor air temperature, heating temperature and mass of additives will be assessed. Finally, further recommendations on future work will be provided in the final part of the paper.

Chapter 2- Literature review

2.01 Frying process

Frying is highly dynamic and complex process that causes severe changes in the food, as well as in the oil due to high temperature, moisture and air [20]. The vegetable oils are mainly composed of fatty acids that have a straight chain aliphatic carboxylic acid structure [21]. Both the carboxyl and unsaturated groups present in fatty acids are very reactive that increases the complexity of understanding the chemical changes in cooking oils. Although evaluation of the changes that take place in oils is challenging, there are three major chemical reactions that can be distinguished in frying oil: hydrolysis, oxidation and thermal alteration. These reactions yield products of different polarity and molecular weight [22]. Table 2-1 summarizes the main groups of new compounds formed in altered oil during frying.

Table 2-1: Main groups of compounds formed during frying [16]

Reactions	Causing agent	Resulting compounds
Hydrolytic alteration	Moisture	Fatty acids
		Monoglycerides
		Diglycerides
		Glycerol
Oxidative alteration	Air	Oxidized monomers, dimers and polymers of TG
		Volatile compounds
Thermal alteration	Temperature	Cyclic monomers
		Nonpolar dimers and polymers

2.02 Hydrolysis

Hydrolysis reactions are one of the simplest reactions in fats and involve breaking ester bonds in the presence of moisture. As a result, diacylglycerides (DG) and free fatty acids (FFA) are formed. The reaction can be followed by the hydrolysis of DG into monoglycerol (MG), FFA and glycerol (Table 2-1). These chemicals are more polar and lighter compared to parent triglycerides (TG). The fatty acids formed after hydrolysis are very reactive and they decompose to yield volatile organic compounds (VOCs) responsible for the desirable and undesirable flavor aspects of the fried food [23]. Saturated free fatty acids, however, are vaporized and removed with steam [22]. Therefore, physical and chemical properties of oils are determined by their fatty acid composition [24].

2.03 Oxidation

As Table 2-1 demonstrates, air causes oxidation of the lipids producing oxidized monomeric, dimeric, and higher oligomeric TG also referred to as oxidized monomers, dimers, and polymers throughout this paper and volatile compounds. Lipid oxidation is generally accepted as a set of classic free radical chain reactions illustrated in following series of reactions [25] involving initiation, propagation and termination reactions.

Firstly, the free radical is formed by spontaneous hydrogen abstraction on an unsaturated fatty acid and it initiates the chain of radical reactions as shown in reaction 2.1. (2.1)

$$L_1H \rightarrow L_1^* \quad (2.1)$$

The initial radical reacts with oxygen and other TGs (L_n) to form new radicals that propagate chain reactions illustrated by reactions 2.2, 2.3, and 2.4.

$$L_1^* + O_2 \leftrightarrow L_1OO^* \quad (2.2)$$

$$L_1OO^* + L_2H \rightarrow L_1OOH + L_2^* \quad (2.3)$$

$$L_2OO^* + L_3H \rightarrow L_2OOH + L_3^* \text{ Etc.} \quad (2.4)$$

High temperature initiates new chains as given in (2.5), to produce alkoxyl and hydroxy radicals.

$$L_nOOH \rightarrow L_nO^* + {}^*OH \quad (2.5)$$

The primary molecular products of the FFA oxidation are proven to be allylic hydroperoxides (LOOH) which are very unstable and they decompose and recombine to terminate radical reactions (Denisov and Afanas'ev 2005; F. Gunstone, et al. 2007). As Figure 2-1 illustrates, the cyclization of the alkoxy radical results in the formation of epoxy, hydroxy and hydroperoxy acids located on one of the unsaturated fatty acids of parent triglyceride. As a result, oxidized monomers with at least one oxygenated group, mainly hydroxy-, epoxy-, keto-groups on at least one of the unsaturated fatty acid are formed [22]. The major characteristics of frying, including high temperature and air, favor polymerization reactions that contribute to the formation of oxidized dimers and oligomers. Due to their heterogeneity, these molecules are polar, and their structure varies significantly, as there can be more than one oxygenated

functions and they can be linked by the C-C bond or by oxygen (C-O-C). However, studies have shown that most polar dimers are C-C linked dimers containing monohydroxy, dihydroxy, and keto groups.

In addition to oxidized compounds that have similar or larger molecular weight compared to parent triglyceride, there are lighter components formed as well. Figure 2-1 demonstrates, the scission of peroxides, that is, the breakdown of LOOH produces aldehydes, alkanes, carboxylic acids, esters and ketones that constitute to a major part of VOCs. The recombination of alkoxy radicals (LO^{*}) yields peroxides and ketones. The scission path of oleic, linoleic, and linolenic acids producing VOCs as a result of oxidation can be found in the Appendices of this work (Appendix A).

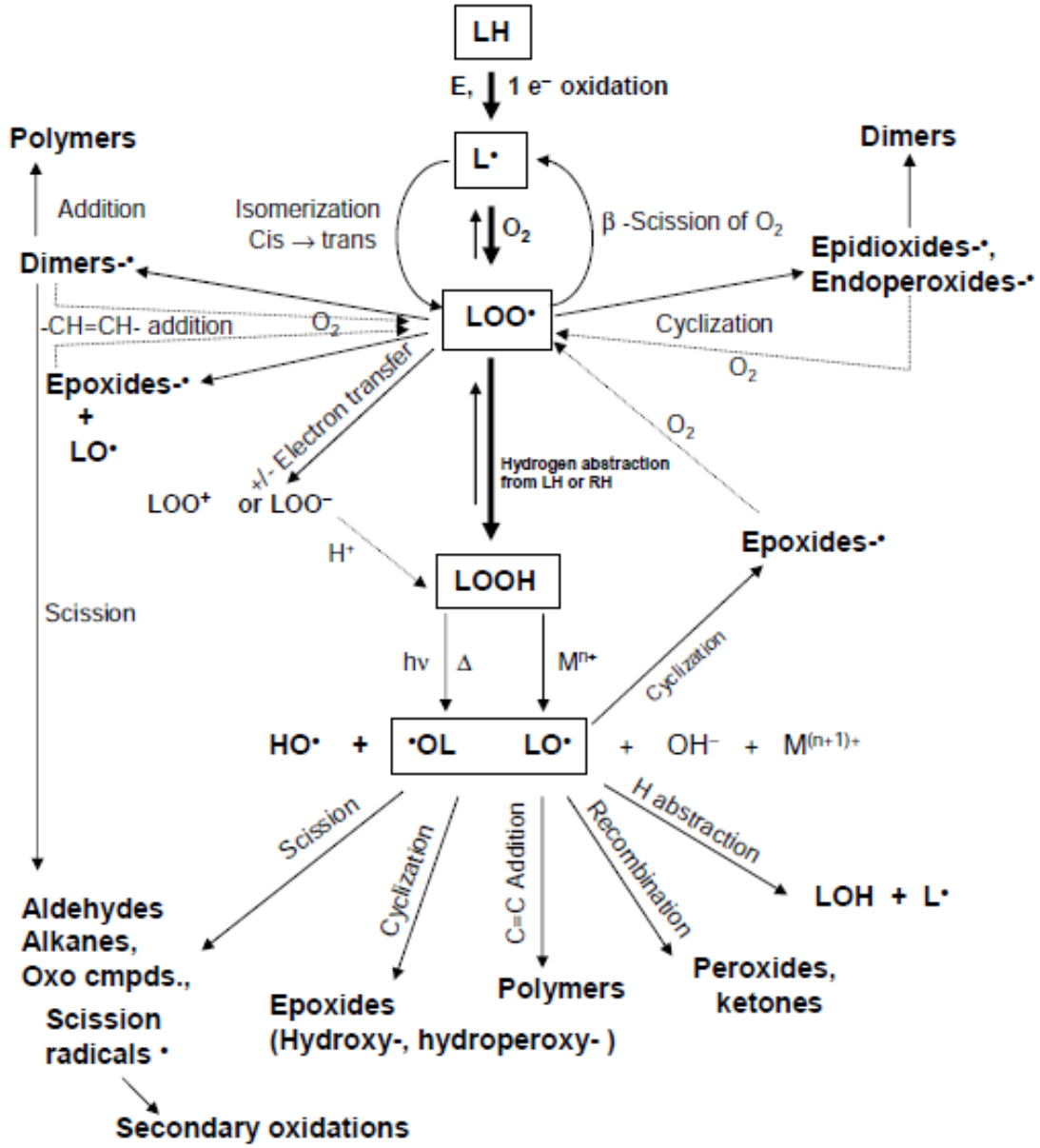

Figure 2-1: Integrated scheme for oil oxidation [8]

It should be noted that at high temperatures scission is favored because thermal energy facilitates bond rupture [25]. Moreover, cyclization producing epoxides is favored when oxygen is limited, and it is less dependent on temperatures, unlike other competing reactions.

Moreover, as Figure 2-2 illustrates, the products obtained as a result of oxidation reaction depend on the time of sample collection, since the

concentration of volatile and non-volatile compounds formed from oil oxidation increase with time.

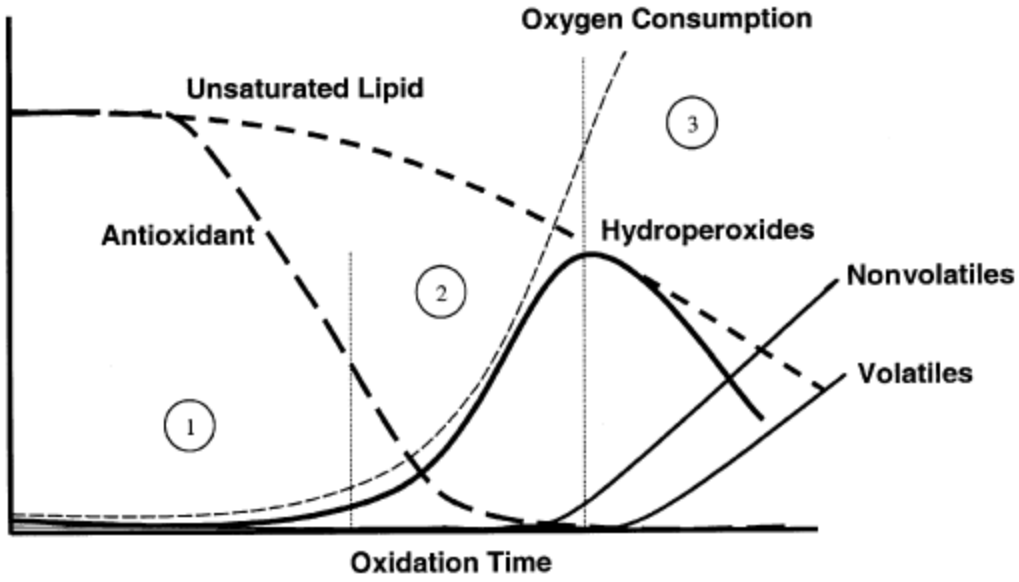

Figure 2-2: The kinetic curve of polyunsaturated fatty acids oxidation [28]

2.04 Thermal alteration

A high temperature of frying operations contributes to the formation of cyclic fatty acids and non-polar dimers. Nonpolar dimers are produced through the interaction of the allyl radicals. The possible routes of nonpolar dimers formation are presented in Figure 2-3.

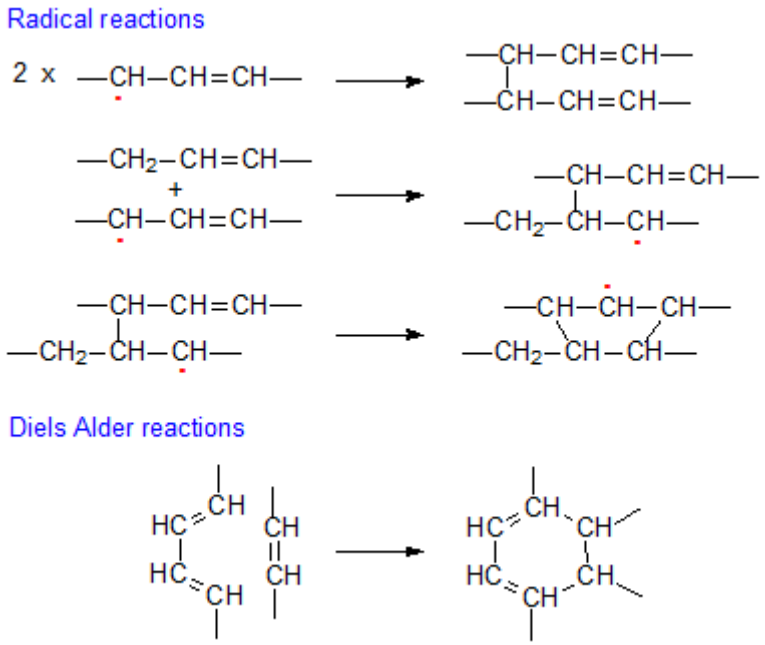

Figure 2-3: Main routes of formation of nonpolar dimers [22]

Figure 2-3 shows that dehydromers are formed by the combination of two allyl radicals. Cyclic nonpolar dimers can be produced by the intermolecular addition of an allyl radical to a double bond followed by the intramolecular addition of an intermediate dimeric radical to a double bond in the same molecule. Another way of cyclic nonpolar dimer formation is Diels-Alder reaction, where the chemical addition, specifically, cycloaddition, between a conjugated diene and an alkene takes place.

When oxygen is limited, isomerization and cyclization reactions involving unsaturated fatty acids take place. As a result, cis- and trans- fats with saturated and unsaturated cyclopentyl and cyclohexyl rings are produced. Figures 2-4, 2-6, and 2-8 demonstrate the carbon atoms involved in the cyclization of linolenic, linoleic, and oleic acids, respectively. These figures show that new cyclic acids

contain five- and six-membered rings, with two substituents – one containing the carboxyl group and the other a hydrocarbon chain [29].

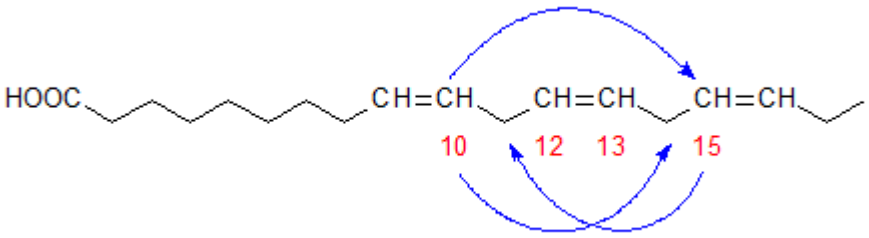

Figure 2-4: Carbon atoms involved in the cyclization of linolenic acid [29]

Referring to Figure 2-4, it is seen that during cyclization one of the double bonds is lost, and the double bond can be within the ring or one of the alkyl chains. Moreover, stereomutation of the double bonds will produce more cis- and trans-isomers.

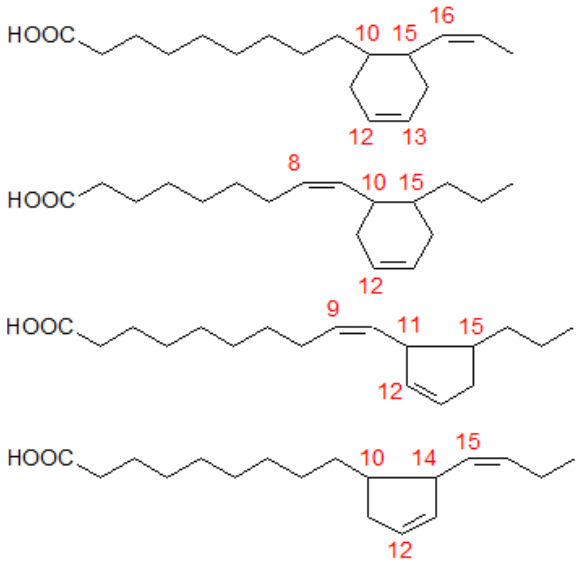

Figure 2-5: Basic structures of cyclic fatty acids formed from linolenic acid [29]

The cyclohexyl group is produced by cyclization between carbons 10 and 15 of the FFA, while cyclopentyl group is produced by cyclization between

carbons 11, 15 and 10, 14, respectively. That is, the cyclization occurs at regions near double bonds only.

Similarly, linoleic and oleic acids also undergo cyclization process near double bonds (Figures 2-6 and 2-8). Interestingly, linoleic acid produces a wider range of cyclic products compared to linolenic acid. For instance, cyclization of linolenic acid results in unsaturated rings, whereas linoleic acid can be cyclized into both saturated and unsaturated 5-membered and 6-membered rings.

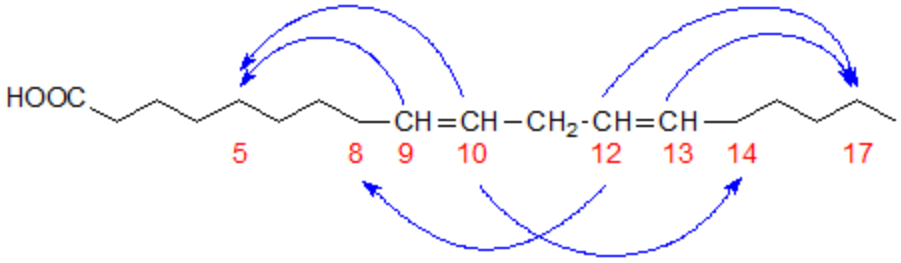

Figure 2-6: Carbon atoms involved in the cyclization of linoleic acid [29]

Moreover, linoleic acid can also be converted into saturated bicyclic acids given in Figure 2-7.

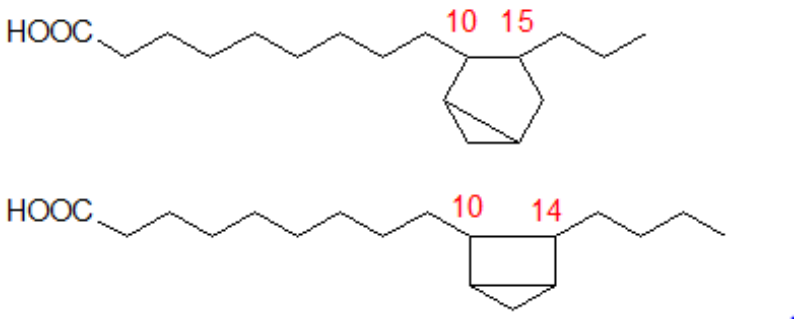

Figure 2-7: Saturated bicyclic acids formed from linoleic acid [29]

Expectedly, due to loss of the double bond, under frying conditions, oleic acid is converted to saturated cyclic fats only following the mechanism shown in Figure 2-8.

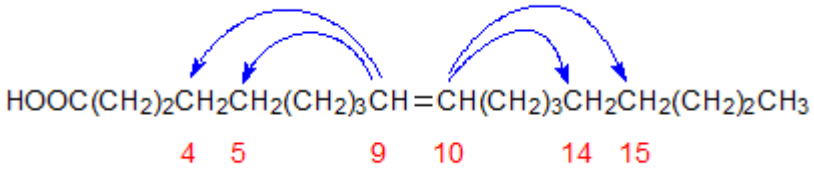

Figure 2-8: Carbon atoms involved in the cyclization of oleic acid [29]

2.05 Methods for estimation of physical parameters.

To choose the method for estimating physical parameters of the components included in the simulation, the following factors should be considered:

- The nature of required properties
- The composition of the mixture
- Operating conditions, including pressure and temperature
- And the availability of parameters

One of the major considerations in this study is Vapor-Liquid equilibrium (VLE) as there are evaporation and condensation taking place. These physical

processes require the use of heat exchangers where the enthalpy and heat capacity of the compounds are necessary for calculations. Additionally, the reactors to mimic the reactions described above require standard enthalpy of formation of pure components.

In this simulation, non-ideal liquid solutions are considered; therefore, activity coefficient models including NRTL, UNIFAC, UNIQUAC were employed to perform VLE calculations. The description of each method is provided in the following subsection.

2.06 NRTL (Non-Random Two-Liquid)

NRTL model is required to estimate the liquid activity coefficients for systems that have a significant deviation from the ideal behavior, which is demonstrated in polar mixtures as in present study [30]. It can be used for vapor–liquid and liquid–liquid equilibria (VLE and LLE) calculations. The general equation of NRTL is given in equation 2.6.

$$ln\gamma_i = \frac{\sum_j x_j \tau_{ji} G_{ji}}{\sum_k x_k G_{ki}} + \sum_j \frac{x_j G_{ji}}{\sum_k x_k G_{ki}} \left(\tau_{ij} - \frac{\sum_m x_m \tau_{mi} G_{mi}}{\sum_k x_k G_{ki}}\right) \quad (2.6)$$

Where γ_i is the activity coefficient of the component, and it is generally greater than 1;

x_j is the mole fraction of the component in the liquid phase;

$\tau_{i,j}$ is dimensionless interaction parameter, notably $\tau_{i,i} = 0$;

Otherwise, it is calculated by equation

$$\tau_{i,j} = a_{ij} + \frac{b_{ij}}{T} + e_{ij}\ln(T) + f_{ij}T \quad (2.7)$$

$$G_{ij} = \exp(-\alpha_{ij}\tau_{ij}) \quad (2.8)$$

With $a_{ij} = c_{ij} + d_{ij}(T - 273.15k)$ (2.9)

c_{ij} has different values depending on the nature of the mixture, for mixtures with immiscible liquids or polar liquid is it 0.2. The binary parameters a_{ij}, b_{ij}, c_{ij}, d_{ij}, e_{ij}, and f_{ij}can be determined from VLE and/or LLE experimental data regression.

2.07 UNIFAC model

UNIFAC model is a group-contribution method, therefore it is predictive. Compared to NRTL it does not require input binary parameters, making it a source of binary interaction data required for NRTL applications. The UNIFAC activity coefficient has combinatorial and residual terms.

$$ln\gamma = ln\gamma_i^c + ln\gamma_i^r \quad (2.10)$$

$$ln\gamma_i^c = \ln\left(\frac{\Phi_i}{x_i}\right) + 1 - \frac{\Phi_i}{x_i} - \frac{Z}{2}\left[\ln\left(\frac{\Phi_i}{\Theta_i}\right) + 1 - \frac{\Phi_i}{\Theta_i}\right] \quad (2.11)$$

Where Φ_i and Θ_i are molecular volume and surface fractions, respectively. They are calculated via equation 2.12 and 2.13, respectively.

$$\Phi_i = \frac{x_i r_i}{\sum_j^{nc} x_j r_j} \quad (2.12)$$

$$\Theta_i = \frac{x_i q_{i\frac{z}{2}}}{\sum_j^{nc} x_i q_{i\frac{z}{2}}} \quad (2.13)$$

Where n_c is the number of components on the mixture;

Z is the coordination number and it is set to 10;

r_i and q_i are calculated by equations 2.14 and 2.15 provided below.

$$r_i = \sum_k^{ng} v_{ki} R_k \quad (2.14)$$

$$q_i = \sum_k^{ng} v_{ki} Q_k \quad (2.15)$$

Where R_k and Q_k are group volume and area parameters, respectively;

v_{ki} is the number of groups of type k in a molecule I; and ng is the number of groups in a mixture.

The residual term $ln\gamma_i^r$ in equation 2.10 is calculated as follows:

$$ln\gamma_i^r = \sum_k^{ng} v_{ki}[ln\Gamma_k - ln\Gamma_k^i] \quad (2.16)$$

Where Γ_k is the activity coefficient of a group at mixture composition;

Γ_k^i is the activity coefficient of group k in a mixture of groups corresponding to pure i.

$$ln\Gamma_k = Q_k \left|1 - ln\sum_m^{ng} \Theta_m \tau_{mk} - \sum_m^{ng} (\frac{\Theta_m \tau_{mk}}{\sum_n^{ng} \Theta_n \tau_{nk}}\right| \quad (2.17)$$

With $\Theta_k = \frac{X_k Q_k \frac{z}{2}}{\sum_m^{ng} X_m Q_m \frac{z}{2}}$ (2.18)

$$\tau_{mn} = e^{-\frac{b_{mn}}{T}} \quad (2.19)$$

The parameter X_k is the group mole fraction of group k in the liquid:

$$X_k = \frac{\sum_j^{nc} v_{kj} x_j}{\sum_j^{nc} \sum_m^{ng} v_{mj} x_j} \quad (2.20)$$

2.08 Modeling and simulation of cooking organic aerosol

2.09 A 3-D Euclidian model

Over the last decades, the interest in COA as significant contributor to airborne particulate matters has increased, and it was included in the US National emission inventory [31]. Nevertheless, current atmospheric chemistry transport model (ACTM) simulations have a tendency to underestimate amount of COA emitted to the atmosphere. To resolve this issue, Ots et al. developed the EMEP MSC-W (European Monitoring and Evaluation Programme Meteorological Synthesizing Centre-West) model that describes the flow of COA over UK as times passes [32]. This 3-D Euclidian model included 21 vertical levels from surface pressure to 0.1 MPa. The 50 km to 50 km resolution was used to perform the calculation in each layer. In this study, a COA tracer was added into the model with dry and wet deposition properties similar to other primary OA components. It was assumed that COA tracer is non-volatile and

does not evaporate into atmosphere. The COA concentrations measured at two sites of London (Marylebone Road and North Kensington) throughout the year served as a base to derive the magnitude and spatial diurnal distributions of COA emissions over the UK.

The evaluation of the COA concentration for two sites demonstrated different results such that the model could simulate COA variation in North Kensington site, but not for Marylebone Road site at measured wind speeds and directions as shown in Figure 2-9.

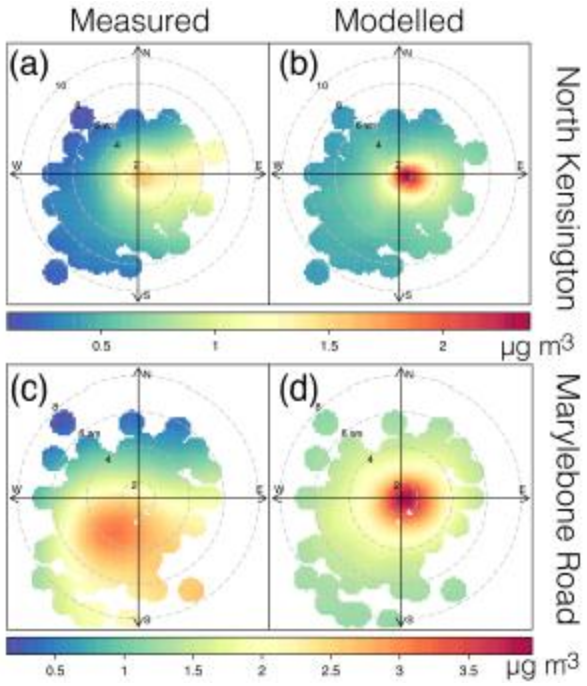

Figure 2-9: Measured (a, c) and modeled (b,d) daily average COA concentrations at different wind speed at North Kensington and Marylebone Road sites. [32]

The source of this deviation was assumed to be a sub-(model-) grid effect at the Marylebone Road site and local air flows. Nevertheless, comparison of the simulation results with the measurement from other locations revealed the diurnal profile of COA emissions from Marylebone Road is more suitable to

simulate COA concentration at centralized urban areas in the UK. Implementation of the models showed that the COA concentration depends on the density of population in the urban area. COA concentrations measured at the central sites of London were 2 times higher than in background sites where the concentration was measured to be 1 $\mu g/m^3$. The average COA concentrations in Manchester, Leeds, and Birmingham were estimated to be approximately 0.6 $\mu g/m^3$, whereas 95% of daily average COA concentrations measured at different sites was between 2-4 $\mu g/m^3$. This showed that model can underestimate the COA concentration in smaller cities, such as Manchester, Leeds, and Birmingham, as it spatially distributes it in 5 km × 5 km grid cells, whereas these cities could be modeled in as a smaller range of grid cells.

2.10 Computer-aided simulation in Aspen Plus

Recently Amouei Torkmahalleh et al. [13] developed a simulation model using Aspen Plus, where the PM emission from heating 6 cooking oils, including soybean, safflower, canola, olive, peanut and sunflower oils was studied. Heating temperatures were below the smoke point of the oils, therefore no reaction in gas and particles phases were considered. It was found that the PM physical properties are affected by the fatty acid composition of the oils. Moreover, by incorporating the common indoor VOCs to the air stream, the importance of existing VOCs in the PM emission rate was seen. This could imply that part of the organic compounds in cooking PM obtained from experimental studies could be related to existing indoor pollutants. Other factors

that affect the PM emission were found to be ambient temperature, relative humidity, heating temperature, and food additives. To be more precise, when salt was added to the oils, PM emission rates reduced similar to experimental results [10].

Chapter 3- Methodology

3.01 General Approach

In this study, a chemical engineering related software, Aspen Plus V9, was employed to simulate the formation of primary organic aerosol (COA) from heated cooking oils at 240 °C. The operating conditions were adapted from experiments published by Liu et al. (2017) including heating temperature (240°C), ambient temperature (21°C) and RH (65%). Sensitivity analysis studies were executed to observe the influence of these parameters on COA formation. Since the temperature of the cooking in this study was higher than smoking point of the corn oil (the temperature at which visible flow of smoke appears above the pan), the simulation includes processes that take place during oil smoking and the subsequent frying, such as hydrolysis, oxidation and thermal alterations, incorporating polymerization, cyclization and pyrolysis reactions. Therefore, the developed model can adequately handle the reactions in the liquid phase (within oil) and gas phase (within cooking emissions), if reaction kinetics and equilibrium constants are available in the literature.

The major constituents of edible oils and fats are triacylglycerols (TAG),

the fatty acid esters of glycerol [21]. Three fatty acids present in the TAG may be identical or different, making vegetable oils a complex mixture of a wide range of chemical compounds. However, in the present study, the vegetable oil is considered as a mixture of triglycerides consisting of the same three fatty acid groups in their backbone for simplicity of analysis [33]. The composition and smoke points of corn, sunflower, and soybean oils are presented in Table 3-1. The values of smoke point for commercial oils can vary drastically due to different free fatty acid composition.

Table 3-1: The composition (wt%) and smoke point of vegetable oils [17]

Fatty acids	Systematic name	Structure*	Formula	Corn	Sunflower	Soybean
Palmitic	hexadecanoic	16:00	$C_{16}H_{32}O_2$	17.7	6	11
Stearic	octadecanoic	18:00	$C_{18}H_{36}O_2$	1.8	6	6
Oleic	cis-9-octadecenoic	18:01	$C_{18}H_{34}O_2$	25.3	18	22
Linoleic	cis-9,cis-12-octadecadienoic	18:02	$C_{18}H_{32}O_2$	54.2	69	53
Linolenic	cis-9,cis-12, cis-15-octadecatrienoic	18:03	$C_{18}H_{30}O_2$	1	1	8
* xx:y indicates xx carbons in the fatty acid chain with y number of double bonds						
Smoke point °C				220±25	209±15	220±20

Indoor air is simulated as a mixture of oxygen and nitrogen together with water, which represents the RH of air.

The water content of the air can be calculated via the following equations.

$$RH = \frac{P_{H2O}}{P^*_{H2O}} \qquad (3.1)$$

Where RH is relative humidity given as fraction;

P_{H2O} is partial pressure of water;

P_{H2O}^{*} is the saturated pressure;

The saturated pressure ($P_{H2O}^{*)}$ is calculated by Antoine's equation, which has the following from:

$$\log_{10} P = A - \frac{B}{C+T} \qquad (3.2)$$

Pressure (P) is calculated in bar, and Temperature (T) is calculated in Kelvin. The coefficients for water are presented in Table 3-2.

Table 3-2: Antoine equation parameters for water [34]

Temperature (K)	A	B	C
273. - 303.	5.40221	1838.675	-31.737

Referring to the Theoretical background section, it is seen that there are two major groups of compounds formed during frying: volatile and non-volatile compounds [35]. These compounds are formed mainly as a result of hydrolysis, oxidation and polymerization reactions. There are thousands of compounds found in altered oil; however, information on the structure and formation of TG polymers, especially that of TG with an oligomerization degree equal to or higher than three, is scant [36]. Consequently, in this simulation, only triglyceride dimers with defined structures were included. Moreover, the volatile organic compounds (VOCs) observed in Liu et al. (2017) were included in the model.

Table 3-3 presents the products expected from heating corn oil at high temperatures. In this study, the VOCs are of main interest, because they are expected to partition into particle phase, and more detailed list of non-volatile chemicals is provided in Appendix B. According to Vo and Morris, glycerol can be defined as volatile, semi-volatile and non-volatile depending on the test methodology applied [37]. Similarly, monoglycerides and fatty acids, that have relatively low molecular weights, can be found in the oil and cooking fumes as well. They were listed as non-volatile in Table 3-3 since they are the products of hydrolysis process occurring in the liquid phase. The numbers in the parenthesis near the compounds represent the number of the chemicals belonging to the given groups used in the simulation.

It should be mentioned that in Aspen Plus, a given process is simulated as steady-state process, while in reality, frying is a highly dynamic process. The simulation presents the results obtained as soon as the operating conditions were established.

Table 3-3: New compounds formed during frying used [2], [16]

Non-volatile organic products		
Hydrolysis products	Oxidation products	Thermal alteration
Fatty acids (5)	epoxy-acids (3)	cyclic acids (18)
Monoglycerides (5)	keto-acids (6)	Non-polar dimers (9)
Diglycerides (5)	Hydroxy-acids (6)	
Glycerol	oxidized dimers (27)	
Volatile organic products		
Theoretical products		Experimental products [2]
pentanal	methyl-oxodecanoate	1-hexanal
nona-1,3-diene	undec-2-enal	ethanal
methylhydroxyheptanoate	dec-2-enal	acrolein
methylhydroxyoctanoate	1-nonanal	propanal
methyloxononanoate	1-octanal	butanal
methyloxodecanoate	1-decanal	methylpyrrole
methyl-heptanoate	1-octanol	pentadienal
methyl-octanoate	1-heptanol	toluene
methyl-nonenoate	1-decene	1,3-cycloheptadiene
methyl-8-oxooctanoate	1-nonene	phenol
1-heptanal	n-octane	xylene
methyl-oxononanoate	n-heptane	benzaldehyde
dimethyl-octanedioate	deca-2,4-dienal	heptenal
Dimethyl- nonanedioate	n-pentane	
methyl-decenoate	non-3-enal	

3.02 Physical properties and thermodynamic models

To estimate the physical properties of pure components and mixtures, Aspen Plus incorporates a variety of physical property models. Aspen Tech. company has adapted all of these correlations into the empirical physical properties of the pure components. A Non-Random Two-Liquid equilibrium (NRTL) model and Ideal Gas Law were applied to predict the phase equilibrium for liquid and vapor phases. The NRTL model was chosen because it considers the molecular structure of the compounds and their polarity. This thermodynamic model needs their binary interactions parameters to estimate the activity coefficients of the liquid phases. Such parameters are found in Aspen

Databases. If interaction parameters are missing in the software, they can be found using various estimating methods such as UNIFAC (UNIQUAC Functional-Group Activity Coefficients) that estimates the activity coefficients in non-ideal systems. It is based on the functional groups present in the compounds and the coefficient corresponding to the strength of interactions.

In Aspen Plus physical properties such as density and viscosity of the liquid mixtures are calculated using the corresponding physical properties of the pure components and their mass/mole fractions in the mixture.

3.03 Defining missing components in Aspen Plus

In this simulation, 137 components describing the composition of air (3), cooking oils (5), volatile (44) and non-volatile compounds (85) produced from heated oil were incorporated. The numbers in parenthesis represent the number of compounds describing the given mixture. Among these, 93 components were missing in Aspen Plus databases and a majority of them are known as non-volatile products that do not partition into the particulate phase. The missing components can be easily introduced to Aspen Plus by importing their structure in a “mol” file that can be downloaded from NIST database (http://webbook.nist.gov/chemistry/), or by entering the molecular structure manually. These structures are vital to estimate required thermophysical properties such as standard enthalpy of formation, critical temperature, critical pressure, etc using estimating structural group methods. The errors associated with estimating methods are unavoidable. However, the scope of this work is the

investigation of volatile organic compounds that partition into particulate phase. Therefore, the errors associated with the estimation methods are assumed to have a negligible effect on the execution of the simulation with regard to COA formation [13].

In this study, the chemical reactions among air molecules and oil under high temperatures were investigated. Therefore, simulation required enthalpy of formation for user-defined components. There are 3 estimation methods that can calculate the standard enthalpy of formation (DHFORM) available in Aspen Plus: Benson, Gani, and Joback. According to Aspen Tech., the Benson method is a second-order group contribution that provides more accurate results compared to Joback method as it accounts for the effect of neighboring atoms[38]. Reported average errors from Benson and Joback methods as

3.7 kJ/mol and 8.9 kJ/mol, respectively. Therefore, in this simulation, Benson method was preferred for estimation of standard enthalpy of formation of pure compounds. Additionally, Aspen Tech states that employing Gani method for complex organic compounds result in less error as it uses contributions from both first-order and second-order groups. The detailed description of these methods is provided in Appendix C of this paper. The analysis of the properties showed that Gani and Joback were unable to estimate the enthalpy of formation for TG dimers and monomers where one of the free fatty acids were altered by the addition of epoxy, keto, or hydroxy groups. A Gani group was chosen for

estimation of DHFORM for TG dimers with C-C or C-O-C linkage as tabulated in Table C-1 in Appendix C.

3.04 Simulation flowsheet

Figure 3-1 shows the frying process flowsheet. Similar flowsheets were developed for all cooking oils. An oil stream named CORN (representative of cooking oils) and air stream named AIR were introduced to an equilibrium reactor (named as HYDRO) and RGibbs reactor (name as TH-OXID mimicking thermal alteration and oxidation reactions). These reactors represent cooking pan to experience phase and chemical equilibria at the given operating conditions. It was assumed that major chemical reactions take place on the surface of the pan; therefore, the air was fed to the reactor at the rate of 0.31 l/min. This value was obtained by multiplying the surface area of the pan ($0.031 m^2$) used by Liu et al. [2] and the depth of oil assigned as 1 cm. The equilibrium reactor requires the stoichiometry of the reactions. The reactions for the hydrolysis process occurring in HYDRO are presented in equations 3.3, 3.4, and 3.5.

$$TG + H_2O \leftrightarrow DG + FFA \tag{3.3}$$

$$DG + H_2O \leftrightarrow MG + FFA \tag{3.4}$$

$$MG + H_2O \leftrightarrow FFA + Glycerol \tag{3.5}$$

Reaction 3.3 represents the decomposition of triglyceride (TG) to diglycerides (DG), which is further decomposed into monoglyceride (MG) and FFA (free fatty acid) as shown in reaction 3.4 and 3.5.

Corn, soybean and sunflower oils are composed of five different triglycerides; consequently, 15 reactions describing the hydrolysis were incorporated. The temperature of HYDRO and TH-OXID reactors was 240 °C, equivalent to the temperature of the oil in the experiments reported by Liu et al. [2]. This temperature is higher than the smoke point of the oil studied in this investigation; therefore, continuous flow of the smoke is expected above the pan. The smoke is the result of volatile organic compounds formation resulting from oxidation and thermal alterations in the vegetable oil [17]. Oxidation and thermal alteration reactions are competitive, that is, they occur at the same time. Consequently, they were represented by the RGibbs reactor (TH-OXID). RGibss yields products by minimizing Gibbs energy of the feed, establishing simultaneous chemical and phase equilibria, at the given operating conditions, including the temperature and pressure. The outputs of the TH-OXID reactor were directed to the flash block (named FLASH), where the Gibbs energy of the input is minimized and two phase split (vapor and liquid) occurs. The vapor fraction of the FLASH block was tuned to obtain the COA emission rate close to the experimental values. The vapor outlet of the flash block (VOC) was then adiabatically mixed with excess air (0.99 m^3/min), and this diluted vapor (stream DL-VOC) was cooled in heat exchanger (COOL) to adjust its temperature to 21 °C. These operations represent rapid dilution and cooling of the cooking fumes above the pan, upon the evaporation. The vapors are assumed to be supersaturated; therefore, it was named SUPSAT. The SUPSAT stream was

duplicated and two streams SUP-A and SUP-B were created. The SUP-B stream was directed to a flash block (PM), where the nucleation of the particles is expected, resulting in three outlets: aqueous aerosol (AOA), organic aerosol (POA) and the vapors that did not partition into particulate phase (VENT). Total PM emission rate is the sum of aerosols enriched with water AOA and with organics POA. To estimate the contribution of solely organic compounds and estimate cooking organic aerosol, the mass flow rate of inorganic compounds was subtracted from POA stream.

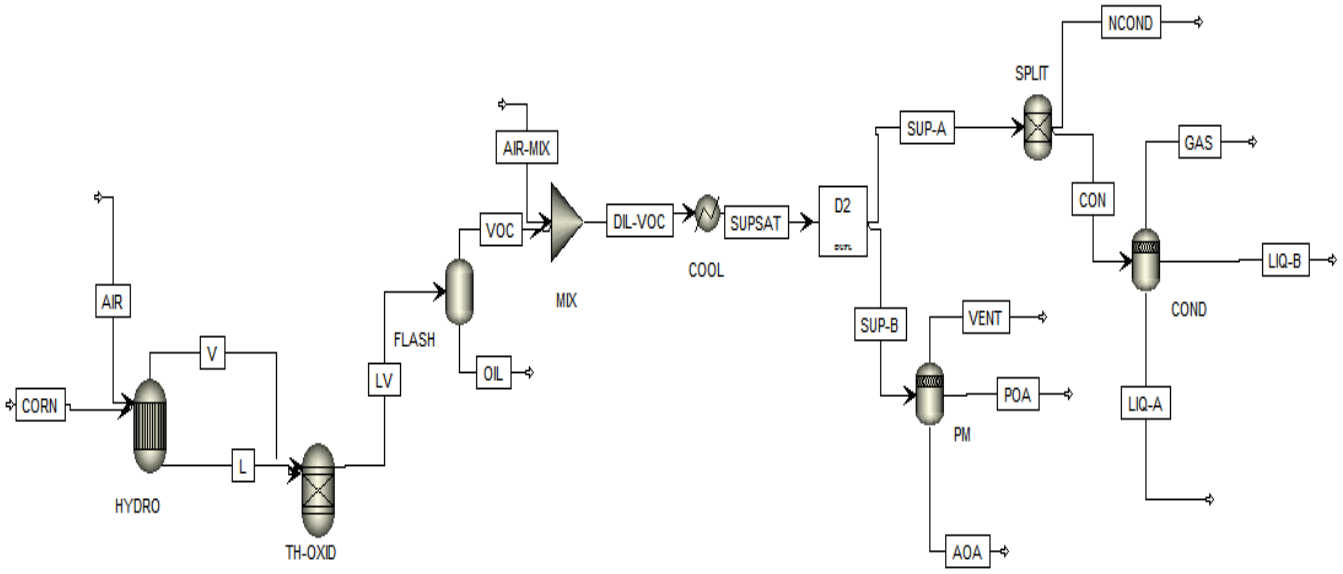

Figure 3-1: The simulation flowsheet-pure oil

3.05 Frying cooking oils mixed with additives

The impact of additives on POA emission was studied by Liu et al [2]. To simulate this experiment, myrcia was mixed with the oils stream (Figure 2-1) before it enters the HYDRO reactor. The mass flow of the myrcia was set as 2

g/min, equivalent to its experimental value reported by Liu et al. [2]. In this simulation, the myrcia was given as liquid oil, and its composition was presented as the volatiles found in essential oils of Myrcia Bracteata [39]. Unfortunately, there are no data that would give the full image of this herb composition, and hence, the compounds found in similar herbs such as diallyl disulfide (DADS), methylpyrrole and aldehydes were included [40]. Moreover, it was revealed that strict quality standards for food safety set by the American Spice Trade Association dictate that spices should contain 10% of water on average [40]. In this study, the composition of myrcia given in Table 3-4 was used. Moreover, the compounds found in cooking emissions from stir-frying myrcia were added to the potential products of TH-OXID reactor including pyrrole, furan, isoprene, 1,3-pentadiene, cyclopentene, pyrroline, 2-butenal, pyrrolidine, pyrazine, monoterpenes (i.e. α-humulene, α-pinene, myrcene and other terpenes with molecular formula $C_{10}H_{16}$), terpenoids (terpenes with functional groups such as α-terpineol, spathulenol) and sesquiterpenes (terpenes with molecular formula $C_{15}H_{24}$ such as a-humulene, g-elemene etc.) [2]. No additional changes to the simulation flowsheet were made.

Table 3-4: Myrcia composition [39]

Component	Chemical Formula	wt%	Component	Chemical Formula	wt%
a-pinene	$C_{10}H_{16}$	4.5	b-elemene	$C_{15}H_{24}$	1
thuja-2,4(10)-diene	$C_{10}H_{14}$	0.1	b-caryophyllene	$C_{15}H_{24}$	1.2
b-pinene	$C_{10}H_{16}$	1.8	g-elemene	$C_{15}H_{24}$	0.7
myrcene	$C_{10}H_{16}$	0.3	aromadendrene	$C_{15}H_{24}$	0.9
p-cymene	$C_{10}H_{14}$	0.4	a-humulene	$C_{15}H_{24}$	0.2
limonene	$C_{10}H_{16}$	0.9	allo-aromadendrene	$C_{15}H_{24}$	0.5
1,8-cineole	$C_{10}H_{18}O$	0.4	g-muurolene	$C_{15}H_{24}$	0.2
g-terpinene	$C_{10}H_{16}$	0.4	ar-curcumene	$C_{15}H_{24}$	0.7
terpinolene	$C_{10}H_{16}$	0.3	bicyclogermacrene	$C_{15}H_{24}$	0.6
p-cymenene	$C_{10}H_{12}$	0.2	a-muurolene	$C_{15}H_{24}$	1.5
exo-fenchol	$C_{10}H_{18}O$	0.2	b-bisabolene	$C_{15}H_{24}$	0.6
a-campholenal	$C_{10}H_{16}O$	0.2	g-cadinene	$C_{15}H_{24}$	0.2
trans-pinocarveol	$C_{10}H_{16}O$	0.5	d-cadinene	$C_{15}H_{24}$	1.1
pinocarvone	$C_{10}H_{14}O$	0.3	trans-calamenene	$C_{15}H_{22}$	0.6
p-mentha-1,5-dien-8-ol	$C_{10}H_{16}O$	0.5	a-calacorene	$C_{15}H_{20}$	1.2
terpinen-4-ol	$C_{10}H_{18}O$	0.3	germacrene b	$C_{15}H_{24}$	8.8
p-methylacetophenone	$C_9H_{10}O$	0.3	spathulenol	$C_{15}H_{24}O$	31
a-terpineol	$C_{10}H_{18}O$	1.3	octanal	$C_8H_{16}O$	0.1
trans-carveol	$C_{10}H_{16}O$	0.2	nonanal	$C_9H_{18}O$	0.1
carvone	$C_{10}H_{14}O$	0.1	methylpyrrole	C_5H_7N	24.3
a-cubebene	$C_{15}H_{24}$	0.4	water	H_2O	10
a-ylangene	$C_{15}H_{24}$	0.4	DADS	$C_6H_{10}S_2$	0.1
a-copaene	$C_{15}H_{24}$	0.4			

The tendency of a component to appear in the vapor phase with regard to particulate phase can be estimated by calculating the ratio of the vapor mole fraction to the liquid mole fraction of that component [13]. This ratio provides the value for the equilibrium ratio or distribution coefficient, referred to as K value. According to Gmehling et al. K values can be evaluated by Raoult's law [41] given in equation 3.6.

$$K_i = \frac{y_i}{x_i} = \frac{P_i^*(T)}{P} \tag{3.6}$$

Where y_i is the mole fraction of the component in the vapor phase, and x_i is the mole fraction in the particulate phase.

In this investigation, the K value was found by dividing the vapor mole fraction of the component in stream VENT to liquid mole fraction in the total particulate phase, consisting of COA and OAO.

3.06 Vapor phase supersaturation

The saturation ratio of the components should exceed 1 to initiate the nucleation process, and partition into the particulate phase [42]. The saturation level of the vapor was calculated by

$$S = \frac{P \sum_i y_i}{P_{dew}} \tag{3.7}$$

Where S is the saturation ratio of the vapor, P is the total vapor pressure, and $\sum_i y_i$ is the sum of mole fraction of the condensable components in the vapor phase. In this study, only oxygen and nitrogen were entered as non-

condensable gases. The calculation of saturation ratio for the individual component is considered as the par of future works. The inputs (the pressure and the sum of the mole fractions of condensable gases) for this equation were adapted from the SUP-A stream (Figure 3-1). In a splitter block (SPLIT), the condensable (CON) and non-condensable (NONCOND) components were separated. The flash block COND processes the CON stream containing only condensable gases at vapor fraction of 0.9999. This vapor fraction ensures the formation of the liquid phase droplet and helps finding the approximate value of the pressure at which the particulate phase forms. This pressure was inserted as P_{dew} in equation 3.7.

In this study, the equation 3.7 was used to calculate the saturation ratio of the gas mixture corresponding to homogeneous nucleation. In the experiment published by Liu et al., the particle size ranged from15 nm to 661 nm [2]. According to McMurry et al., new particle production, i.e. heterogeneous nucleation, is observed when stable molecular clusters formed from the gas phase grow and reach a detectable size before they are scavenged by preexisting particles [43]. The minimum detectable size for aerosol particles is about 3 nm, that is, in this simulation, COA was assumed to be produced from the heterogeneous nucleation.

Moreover, in this simulation, new thermodynamic phase formed as a result of nucleation is liquid phase, whereas the formation of solid particulates was not considered due to limitations of NRTL to calculate solid-liquid

equilibrium. Noteworthy, the equation quantifies the saturation ratio of volatile organic compounds and water, forming a mixture of 45 components. However, it can also be implemented to estimate saturation ratio for mixtures with different compositions.

To summarize, in this simulation study, the following assumptions were made:

- There are perfect mixing and uniform heat distribution on over the pan surface.
- The total aerosol is formed as a result of heterogeneous nucleation.
- Chemical reactions take place on the surface of the pan, as they require presence of oxygen and water.

3.07 FLASH vapor fraction tuning

The vapor fraction of the flash block FLASH was tuned to obtain the POA emission rate that matches the experimental POA emission rate value for corn oil. The POA emission rate from heating corn oil was reported by Liu et al [2] without particle size distribution. In the reference experiment, only the concentration of the POA was given, and it should be converted into mass flow rate, to make a basis for the model validation. Liu et al. calculated the emission rate of POA by the equation 3.8 [2]

$$ER = \frac{[OA] \times DR \times F}{M_{spice}} \tag{3.8}$$

Where ER is the POA emission rate;

[OA] is the aerosol concentration;

DR is the dilution ratio; in the experiment it was reported as approximately 22;

F is the flow rate of the carrier gas in m^3/min;

M_{spice} is the mass of the additive in g.

The tuning of the vapor fraction of the FLASH was conducted and the emission rate matched that of the experiments. The minimum deviation from the experimental value is obtained at vapor fraction of 0.1717.

Chapter 4- Results and Discussion

4.01 Model Validation

The current simulation was conducted based on the experimental study published by Liu et al. [2]. They reported the composition of the volatile organic compounds (VOCs) and the concentration of primary organic aerosol (POA) produced from frying with corn oil. The reported POA concentration was 42 $\mu g/m^3$, and using the equation 3.8, estimated and simulated POA emission rate is 9.24×10^{-4} g/min.

To validate VOC composition, it is important to emphasize that a VUV-SPI-TOFMS (SPIMS-1000, Guangzhou Hexin Analytical Instrument Co., Ltd) was used in the experimental study of Liu et al. to characterize VOC emissions [2]. However, this analysis was unable to differentiate isomers as well as isobaric compounds [44] [45]. That is, it cannot differentiate the molecules with identical molecular weight but with different atoms from each other. Therefore, although it was assumed that only butanal was emitted from corn oil [2], it could be pentane as well. Glycerol and toluene also have identical molecular weight (92) that may biase the analyses.

The composition of the smoking process products and altered oil obtained in the simulation is tabulated in Table 4-1. The components marked by asterisk* were reported by Liu et al. as well [2]. The VOC emissions from heating corn

oils were dominated by light aldehydes, including ethanal, propanal and butanal, showing consistency with the experimental data. Since the molecular weights of pentane and butanal are identical, pentane could be dominating compound as well. Moreover, both the experiment and simulation showed the abundance of cycloheptadiene and toluene in cooking fumes. In contrast to experimental data, the model included acrolein, a common component of VOC from cooking oils [46], [47], [48] and did not include xylene and benzaldehyde. Additionally, free fatty acids such as palmitic and stearic acids, glycerol were observed, although they were not reported by Liu et al. [2]. This discrepancy between the experimental and simulation components could be due to no report on the compounds with molecular weight more than 204 g/mol.

Overall, Liu et al. reported 9 compounds in the VOCs emitted from heated corn oil. In this simulation study, 39 volatile compounds were observed in the output of TH-OXID reactor, among which 8 matched experimental data. Good replication of the empirical VOC composition COA emission rates show that the model can adequately replicate the frying processes.

Table 4-1: The composition of chemical alteration products formed from frying corn oil (both liquid and vapor phase) from the simulation

Components	Mass fraction	Components	Mass fraction
Ethanal*	0.354	Oleic acid	2.29×10^{-14}
Cycloheptadiene*	0.2422	Decadiene	4.31×10^{-18}
Pentane	0.237	Linoleic acid	1.29×10^{-19}
Stearic acid	0.231	Monopalmitin	8.13×10^{-23}
Propanal*	0.01634	Monostearin	2.25×10^{-24}
Toluene*	0.00417	Linolenic acid	1.95×10^{-24}
Palmitic acid	0.00164	Cyclic linoleic acid	1.16×10^{-27}
Heptane	1.291×10^{-3}	Oxidized triolein monomer with	1.14×10^{-27}

		keto group	
Butanal*	0.00087	Monoolein	3.01×10^{-27}
Acrolein	2.30×10^{-4}	Cyclic linolenic acid	1.10×10^{-27}
Octane	0.0001	Cyclic oleic acid	1.10×10^{-27}
Pentanal	5.79×10^{-5}	Tripalmitin	1.97×10^{-27}
Hexanal	6.53×10^{-6}	Oxidized trilinolein dimer	9.36×10^{-28}
		Oxidized trilinolein monomer with	
Methyl heptanoate	5.35×10^{-6}	hydroperoxy group	5.29×10^{-27}
Heptenal*	4.16×10^{-7}	Monolinolein	1.71×10^{-27}
Heptanal	6.77×10^{-8}	Diolein	1.58×10^{-27}
Octanol	2.87×10^{-8}	Oxidized triolein dimer	1.87×10^{-27}
		Oxidized trilinolein monomer with	
Methyl octanoate	2.49×10^{-8}	keto acid	2.93×10^{-27}
Glycerol	1.49×10^{-8}	Trilinolenin	1.16×10^{-27}
Octanal	9.79×10^{-9}	Distearin	1.14×10^{-27}
Nonene	4.41×10^{-9}	Trilinolein	1.11×10^{-27}
		Oxidized triolein dimer with keto	
Dimethyl-octadiene	6.23×10^{-10}	group	5.36×10^{-27}
Nonanal	6.04×10^{-10}	Monolinolenin	5.21×10^{-27}
Methylhydroxyheptanoate	1.88×10^{-10}	Trilinolenin dimer	5.03×10^{-28}
		Oxidized trilinolein dimer with keto	
Methyl-8-oxooctanoate	1.67×10^{-10}	group	9.85×10^{-28}
Decene	1.18×10^{-10}	Triolein dimer	8.01×10^{-28}
		Oxidized trilinolein monomer with	
Decanal	4.87×10^{-11}	epoxy group	2.38×10^{-28}
dimethyl nonanedioate	4.85×10^{-11}	Trilinolein dimer	3.19×10^{-28}
Methyl-oxononanoate	1.31×10^{-11}	Tristearin	6.25×10^{-29}
		Oxidized triolein monomer with	
methyloxononanoate	1.31×10^{-11}	hydroxy group	4.76×10^{-29}
methylhydroxyoctanoate	1.25×10^{-11}	Dilinolein	3.47×10^{-29}
Nonenal	6.96×10^{-12}	Oxidized triolein dimer	1.29×10^{-29}
Methylpyrrole*	5.02×10^{-12}	Oxidized triolein monomer	1.25×10^{-29}
Pentadienal*	1.44×10^{-12}	Oxidized trilinolenin monomer	8.56×10^{-28}
		Oxidized trilinolein monomer with	
Methyloxodecanoate	1.00×10^{-12}	dihydroxy group	3.04×10^{-28}
		Oxidized trilinolein dimer with keto	
Decenal	7.00×10^{-13}	group	1.69×10^{-28}
Nonadiene	1.09×10^{-13}	Triolein	3.36×10^{-30}
Methyl-nonenoate	7.70×10^{-14}	Dilinolenin	2.28×10^{-30}
Undecanal	2.51×10^{-14}	Dipalmitin	2.27×10^{-30}

The presence of the fatty acids in the VOC showed a good correlation with the theoretical predictions. To be more precise, the mass fractions of

saturated fatty acids prevail over unsaturated fatty acids, as latter ones undergo thermal oxidation reactions.

In addition to VOCs, the output from the TH-OXID reactor contains non-volatile products formed in altered oil. As Table 4-1 demonstrates, the amount of non-volatile compounds is significantly lower than VOC. That is, a major fraction of oil underwent oxidation and thermal alteration reactions and vaporized. The vapor fraction of the stream leaving the TH-OXID reactor was 0.97, which is higher than expected. However, at high temperatures the scission reactions producing short-chain compounds are favored compared to the addition and polymerization reactions as given in the Theoretical background section. Another explanation of high vapor fraction could be the input composition of the corn oil, where unsaponifiable matter, including sterols, triterpenes and triterpene alcohols, tocopherols were included in the oil composition [49]. The presence of the tocopherols increases the oxidative stability of the oil, making it less susceptive to chemical alterations, and thus, it promotes producing less VOCs. Furthermore, the input to the TH-OXID reactor included only non-volatile components with known structure. Therefore, introducing more polymeric compounds could result in lower vapor fraction of the total cooking emissions. Among oxidized monomers, oxidized dimers and non-polar dimers of triglycerides altered triolein, trilinolein and trilinolenin monomers with one cyclized fatty acid were dominant over others. This observation could be due to the limited amount of oxygen supplied to the

reactors, because cyclization reactions are preferred at oxygen-limited systems [21]. It should be noted that the higher weight products including oxidized triglyceride monomers, oxidized TG dimers, non-polar dimers and cyclized TG monomers were grouped depending on the type of the alteration. Cyclic linoleic acid, for instance, represents 10 different trilinolein with various 5- and 6-membered rings formed. Amongst the trilinolein cyclic monomers, the fatty acids with unsaturated 5-membered ring dominated over the cyclized linoleic acids with saturated 5-membered ring and 6-membered ring by an order of magnitude. Moreover, dimerization and oxidation reactions did not appear to be selective in terms of the allylic position where reaction occurs.

As the model was validated, this model was employed to investigate the COA formation during frying soybean and sunflower oils. The compositions of individual non-volatile components are provided in the Appendices.

4.02 Composition and emission rate of POA from frying oils.

The POA compositions resulted from frying three individual oils at 240 °C are presented in Table 4-2 . It should be emphasized that the mass flow rates of water, oxygen and nitrogen were subtracted from the total particulate matter (PM) to obtain COA emission rate, as they are inorganic. In other words, water, as well air components contribute to the formation of PM, but the scope of the work is simulating COA formation. It was found that POA emission rates from frying soybean and sunflower oils are 0.089 g/min and 0.092 g/min, respectively. These POA emission rates are greater than POA emitted from corn

oil by two orders of magnitude. The possible explanation of such increase in COA is the vapor fractions of the streams leaving the TH-OXID reactor that was estimated to be 1 that significantly increases the amount of VOC partitioning to the particulate phase. Moreover, the unsaturated free fatty acid compositions of soybean and corn oils are higher (83% and 82%, respectively), suggesting that they possess less oxidative stability compared to corn oil (81.5%). The smoke point of the sunflower oil is usually lower than that of the soybean oil, resulting in higher amount of VOCs emitted that further condensed to form COA. This argument can be also supported by the compositions of acrolein in three oils, being highest in sunflower oil and lowest in corn oil, as this compound is responsible for the smell of the smoke emitted from heated oils. However, in the experimented conducted by Amouei Torkmahalleh et al., it was found that heating soybean oil results in higher PM formation compared to sunflower oil [9]. It should be noted, however, that the compositions of commercial oils vary depending on the producers, because the food producer has full responsibility for the choice of suitable antioxidants according to the corresponding guidelines governed by regulatory laws of the individual country or the international bodies that declare their safety [50]. Thus, the same vegetable oil from various producers can emit different amounts of PM.

As shown in Table 4-1 cycloheptadiene was the dominant compound in the COA emitted from all frying oils followed with ethanal. Noteworthy, in VOCs of all three oils, the component with the highest composition was ethanal

(Appendix D). This phenomenon could be attributed to the tendency of a component to appear in the vapor phase relative to particulate phase that can be represented by the equilibrium ratio (K value). At K values more than1, the component tends to appear in the vapor phase, whereas the K values less than 1 demonstrate that the component's tendency to be present in the particulate phase. As Table 4-3 shows cycloheptadiene has a K value (0.021) which is smaller than K value of ethanal (2.16-2.17) by two orders of magnitude. That is, cycloheptadiene is more abundant in vapor phase than ethanal; and the composition of the VOCs from cooking and POA are not identical as shown in Table D-1 in Appendices.

Table 4-3 shows that the K value of an individual component is similar in different oils. Nonanal, decanal, decene, methylhydroxyheptanoate, methyl-8-oxooctanoate, dimethyl nonanedioate and pentadienal that were found in the COA emitted from soybean and sunflower oil, however they did not contribute to COA from heated corn oil. All of the saturated fatty acids had K values significantly lower than 1, implying that they favor the PM. By fact, palmitic and stearic acid have the lowest values of K, compared to other compounds and this finding can be explained by relatively high molecular weight of the palmitic and stearic acids, 256.4 g/mol and 284.5 g/mol, respectively. Although glycerol is a light compound, it showed higher tendency to condensate, compared to other VOCs. Although the K value of aldehydes ($C \geq 2$, including unsaturated aldehyde acrolein), alkanes (octane, heptane, pentane), alkenes (nonene), and

toluene exceeded 1, they appeared in PM phase due to supersaturation of VOC mixture.

Table 4-2: POA composition (mass fraction) generated by frying oils

Components	Corn	Soybean	Sunflower
Cycloheptadiene	0.891	0.957	0.958
Ethanal	0.109	0.043	0.042
Propanal	4.96×10^{-4}	2.36×10^{-4}	2.31×10^{-4}
Butanal	3.80×10^{-5}	2.12×10^{-5}	2.07×10^{-5}
Acrolein	1.72×10^{-5}	1.08×10^{-5}	1.07×10^{-5}
Stearic acid	2.75×10^{-5}	3.48×10^{-8}	3.60×10^{-8}
Palmitic acid	6.60×10^{-6}	8.53×10^{-10}	7.23×10^{-10}
Pentane	3.50×10^{-6}	2.35×10^{-6}	2.27×10^{-6}
Toluene	1.72×10^{-6}	3.10×10^{-6}	3.16×10^{-6}
Pentanal	1.01×10^{-6}	7.60×10^{-7}	7.42×10^{-7}
Methyl-9-oxononanoate	1.18×10^{-7}	7.47×10^{-8}	7.25×10^{-8}
Heptenal	5.54×10^{-8}	7.24×10^{-8}	6.94×10^{-8}
Hexanal	4.14×10^{-8}	3.88×10^{-8}	3.78×10^{-8}
Methyl heptanoate	2.85×10^{-8}	4.74×10^{-8}	4.65×10^{-8}
Heptane	7.72×10^{-9}	9.70×10^{-9}	9.40×10^{-9}
Glycerol	5.48×10^{-9}	3.21×10^{-9}	3.08×10^{-9}
Octanol	1.82×10^{-9}	3.78×10^{-9}	3.64×10^{-9}
Octane	1.71×10^{-9}	2.33×10^{-9}	2.26×10^{-9}
Heptanal	1.59×10^{-10}	1.92×10^{-10}	1.88×10^{-10}
Octanal	1.34×10^{-11}	2.25×10^{-11}	2.19×10^{-11}
Methyl hydroxyheptanoate	0	1.02×10^{-10}	9.90×10^{-11}
Methyl-8-oxooctanoate	0	3.07×10^{-11}	3.04×10^{-11}
Dimethyl nonanedioate	0	8.13×10^{-11}	8.06×10^{-11}
Nonene	6.17×10^{-13}	3.16×10^{-12}	3.14×10^{-12}
Decanal	0	2.82×10^{-12}	2.76×10^{-12}
Nonanal	0	1.21×10^{-12}	1.18×10^{-12}
Pentadienal*	0	4.99×10^{-12}	5.02×10^{-12}
Decene	0	2.94×10^{-13}	2.93×10^{-13}

Table 4-3: K values for various compounds found in the PM of vegetable oils.

Components	Corn	Soybean	Sunflower
Oxygen	773.8724	772.6396	772.6239
Nitrogen	1159.248	1156.575	1156.537
Water	0.012114	0.012114	0.012114
Acrolein	5.807262	5.513383	5.508205
Palmitic acid	2.01×10^{-12}	3.66×10^{-12}	3.7×10^{-12}
Stearic acid	1.24×10^{-15}	3.37×10^{-15}	3.42×10^{-15}
Glycerol	2.06×10^{-8}	2.06×10^{-8}	2.06×10^{-8}
Nonanal		7.245833	7.1895
Octanal	12.36472	9.311496	9.264302
Decanal		0.181473	0.179367
Octanol	0.127983	0.085872	0.085271
Heptenal	0.121475	0.099929	0.099579
Decene		9.681317	9.391321
Nonene	259.1303	51.42298	50.14574
Octane	3459.775	1808.587	1788.23
Heptane	16990.08	8390.622	8288.33
Hexanal	8.651039	7.823092	7.808782
Pentane	25075.78	17439.91	17327.52
Pentanal	6.434633	6.064111	6.05755
Methylhydroxyheptanoate		0.000575	0.000573
Methyl heptanoate	3.998665	2.363587	2.342221
Methyl-9-oxononanoate	0.000155	0.000155	0.000155
Methyl-8-oxooctanoate		0.027997	0.027841
Heptanal	12.24196	10.35225	10.32089
Dimethyl nonanedioate		0.01407	0.013936
Ethanal	2.181468	2.164918	2.164629
Propanal	14.311	13.33423	13.31725
Butanal	4.777465	4.321043	4.313268
Pentadienal		0.037323	0.037323
Toluene	147.7519	121.2612	120.8278
Cycloheptadiene	0.021479	0.021465	0.021465

4.03 Effect of indoor air temperature

Figure 4-1 presents POA emission rate from heating corn oil at different indoor temperatures. POA emission rate appeared to decrease with increasing indoor air temperature. As seen in Figure 4-1, the POA emission rate has drastically decreased when the temperature of PM flash separator representing the nucleation process was changed to 20 °C. The POA emission rates at temperatures higher than 10 °C had an order of -8; therefore, visually POA emission rate appears as zero. This sudden decrease in the COA emission rate could be related to the saturation ratio of the vapors that varies with temperature. In equation 3.7 dew pressure is the function of temperature; it decreases with temperature. That is, there is a temperature at which the first droplet of PM is formed from supersaturation of vapor mixture. To find it, the temperature of AIR-MIX stream was changed, and the temperature of diluted vapor stream was recorded. Obtained temperature values were inserted to COND flash block to define the pressure at which 0.00001 liquid fraction is achieved. As a result, Figure 4-2 was obtained.

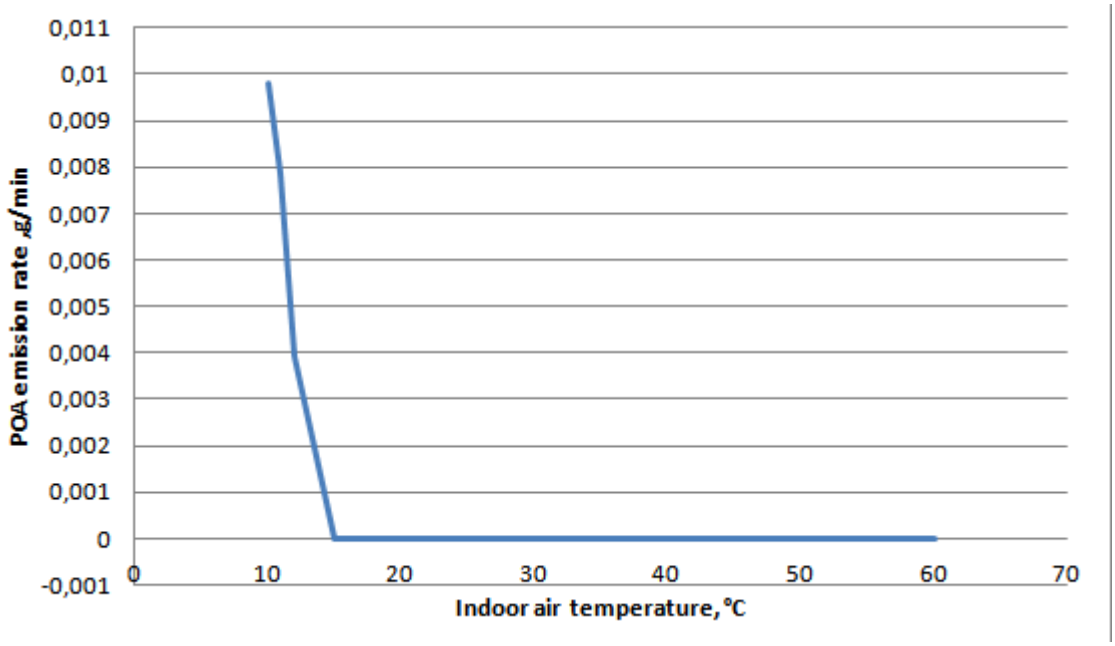

Figure 4-1: The POA emission rate variation with air temperature

As Figure 4-2 shows saturation ratio decreases with temperature above the pan. During the experiment published by Liu et al. [2] no nucleation on the pan surface was observed, and results of the simulation also showed that at the pan surface, where temperature of the fumes is 240 °C saturation ratio of vapors is equivalent to 0.0025 and nucleation of particles could not take place. There is a definite height where the temperature of diluted VOCs is sufficiently low to initiate the nucleation of particles. When temperature of the diluted vapors reached 36 °C, the saturation ratio reached 1, corresponding to a minimum height where COA can be observed.

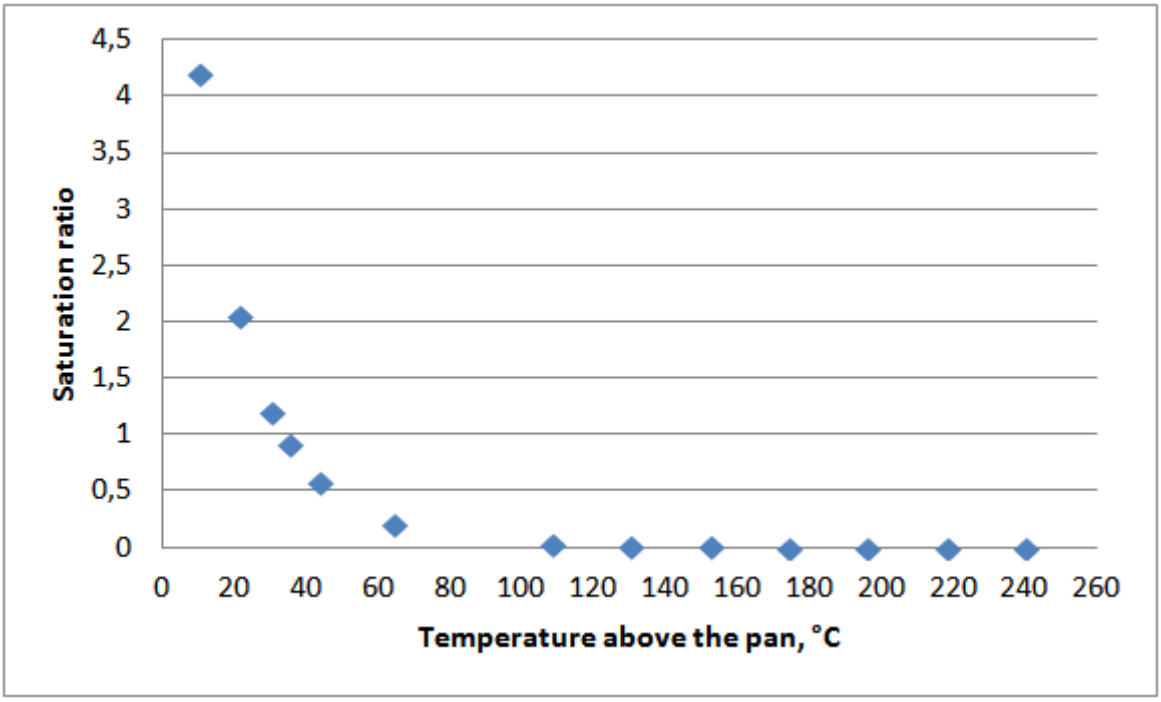

Figure 4-2: Saturation ratio variation with temperature above the pan

Table 4-4 presents PM density and viscosity resulted from heated corn oil at 240 °C at different indoor temperatures. Density of PM decreased with temperature, while increases in the PM viscosity until 30 °C was observed, but then reduction in viscosity was registered at higher temperature than 30 ^{o}C. These variations in physical properties were related to the composition of total PM produced from frying oils provided in Table 4-5.

Table 4-4: Physical properties of PM at different indoor temperature

Temperature, °C	Density, kg/m^3	Viscosity, N*sec/m^2
10	1007.91	0.0013
20	828.059	0.00255
30	818.59	0.00584
40	812.256	0.00565
50	805.187	0.00477

At 10 °C, the PM emitted from heating corn oil above its smoke point was dominated by water, as at this temperature its equilibrium constant was

significantly lower than for others. The density of water at 10 °C is equivalent to 997 kg/m^3 and density of PM was estimated to be 1007.91 kg/m^3 implying that density of PM is governed by the component with highest mass fraction in the mixture. Similarly, at 20 °C the major component in the PM was stearic acid with density of 840 kg/m^3. Increase in indoor air temperature was followed by a reduction in water contribution to PM resulting in lower density values. The change in the viscosity values was correlated with the contribution of palmitic acid, methyl-oxo-nonanoate, glycerol, octanal, octanal, heptenal, octane, hexanal, pentane, pentanal, heptanal and toluene to PM. As Table 4-5 presents the mass fractions of these compounds increased before the temperature reached 30 °C, and then decreased.

As Table 4-5presents, the compositions of PMs are sensitive to the change of indoor air temperature, such that the contribution of water to PM decreases with temperature. The increase from 10 °C to 20 °C resulted in approximately 10 times reduction of water mass fraction in PM. Further increase in ambient air temperature decreased the water mass fraction. Therefore, it is concluded that the absorption of water by aerosol particles is higher at lower indoor air temperatures. As a result, the effect of water on the physical and chemical properties of aerosol decreases with temperature[51]. According to Ansari and Pandis, the presence of water changes the partitioning of semivolatile species between the gas and aerosol phase and affects the particle composition that explains the variation is PM compositions at different indoor temperatures [52].

As aerosol water provides a medium for heterogeneous chemical reactions in the atmosphere, there are potential chemical reactions occurring in particulate phase resulting in different compositions.

Table 4-5: Composition of PM emitted from heating corn oil at different indoor temperatures

Components	10°C	20°C	30°C	40°C	50°C
Oxygen	0.00047	0.02058	0.02148	0.02147	0.02169
Nitrogen	0.00105	0.00029	0.00025	0.00027	0.00033
Water	0.99817	0.10418	0.0138	0.00584	0.00361
Acrolein	1.44×10^{-10}	2.20×10^{-10}	1.44×10^{-10}	7.40×10^{-10}	4.81×10^{-11}
Palmitic acid	1.91×10^{-9}	0.1523	0.15511	0.09919	0.03241
Stearic acid	8.98×10^{-9}	0.72247	0.8093	0.8732	0.94195
Glycerol	8.94×10^{-11}	2.38×10^{-6}	7.04×10^{-7}	1.69×10^{-7}	5.22×10^{-8}
Octanal	1.06×10^{-14}	1.76×10^{-11}	2.20×10^{-11}	1.14×10^{-11}	6.32×10^{-12}
Octanol	2.49×10^{-12}	7.34×10^{-9}	2.76×10^{-9}	8.43×10^{-10}	3.31×10^{-10}
Heptenal	6.19×10^{-11}	3.40×10^{-8}	1.67×10^{-8}	5.10×10^{-9}	2.06×10^{-9}
Octane	1.08×10^{-12}	1.58×10^{-8}	2.00×10^{-8}	1.13×10^{-8}	6.96×10^{-9}
Heptane	3.76×10^{-12}	7.52×10^{-8}	9.00×10^{-8}	5.14×10^{-8}	3.27×10^{-8}
Hexanal	2.03×10^{-11}	6.53×10^{-10}	1.44×10^{-9}	8.86×10^{-10}	5.59×10^{-10}
Pentane	1.14×10^{-9}	4.48×10^{-7}	7.97×10^{-7}	4.49×10^{-7}	2.81×10^{-7}
Pentanal	4.02×10^{-10}	2.73×10^{-9}	5.74×10^{-9}	3.55×10^{-9}	2.29×10^{-9}
Methylhydroxyheptanoate	5.94×10^{-11}	4.12×10^{-7}	1.05×10^{-7}	2.80×10^{-8}	1.04×10^{-8}
Methylhydroxyoctanoate	2.28×10^{-12}	1.21×10^{-7}	2.63×10^{-8}	6.58×10^{-9}	2.26×10^{-9}
Methyl-oxononanoate	6.24×10^{-13}	3.79×10^{-9}	1.44×10^{-9}	4.85×10^{-10}	2.04×10^{-10}
Methyl heptanoate	1.30×10^{-8}	1.55×10^{-5}	9.03×10^{-6}	4.02×10^{-6}	2.11×10^{-6}
Methyl octanoate	1.01×10^{-7}	1.00×10^{-7}	1.91×10^{-8}	7.15×10^{-9}	3.70×10^{-9}
Methyl nonanoate	9.81×10^{-13}	1.43×10^{-9}	4.78×10^{-10}	1.56×10^{-10}	6.65×10^{-11}
Methyl-8-Oxooctanoate	7.73×10^{-12}	1.22×10^{-8}	5.73×10^{-9}	2.10×10^{-9}	9.50×10^{-10}
Heptanal	7.08×10^{-14}	1.45×10^{-11}	2.73×10^{-11}	1.62×10^{-11}	9.93×10^{-12}
Methyl-Oxononanoate	6.24×10^{-13}	3.79×10^{-9}	1.44×10^{-9}	4.85×10^{-10}	2.04×10^{-10}
Dimethyl octanedioate	1.62×10^{-8}	0.00011	4.10×10^{-5}	1.42×10^{-5}	6.12×10^{-6}
Dimethyl nonanedioate	1.79×10^{-9}	3.27×10^{-5}	1.01×10^{-5}	3.24×10^{-6}	1.30×10^{-6}
Ethanal	3.47×10^{-5}	2.11×10^{-6}	1.14×10^{-6}	7.54×10^{-7}	5.88×10^{-7}
Propanal	1.14×10^{-7}	8.33×10^{-8}	7.76×10^{-8}	4.84×10^{-8}	3.57×10^{-8}
Butanal	1.13×10^{-8}	7.66×10^{-9}	5.89×10^{-9}	3.76×10^{-9}	2.76×10^{-9}
Toluene	1.44×10^{-9}	2.05×10^{-8}	5.78×10^{-8}	4.40×10^{-8}	3.31×10^{-8}
Cycloheptadiene	0.00028	1.59×10^{-5}	3.98×10^{-6}	1.92×10^{-6}	1.25×10^{-6}

4.04 Effect of heating temperature

The simulation showed that POA emissions increased with heating temperature, as the amount of VOCs produced from heating corn oil increased. As Figure 4-3 shows increase in POA emission rate is almost linear starting from 180 °C. Table 4-6 provides the numerical values for the POA emission rate at different corn oil temperatures and increment factor compared to lower temperature.

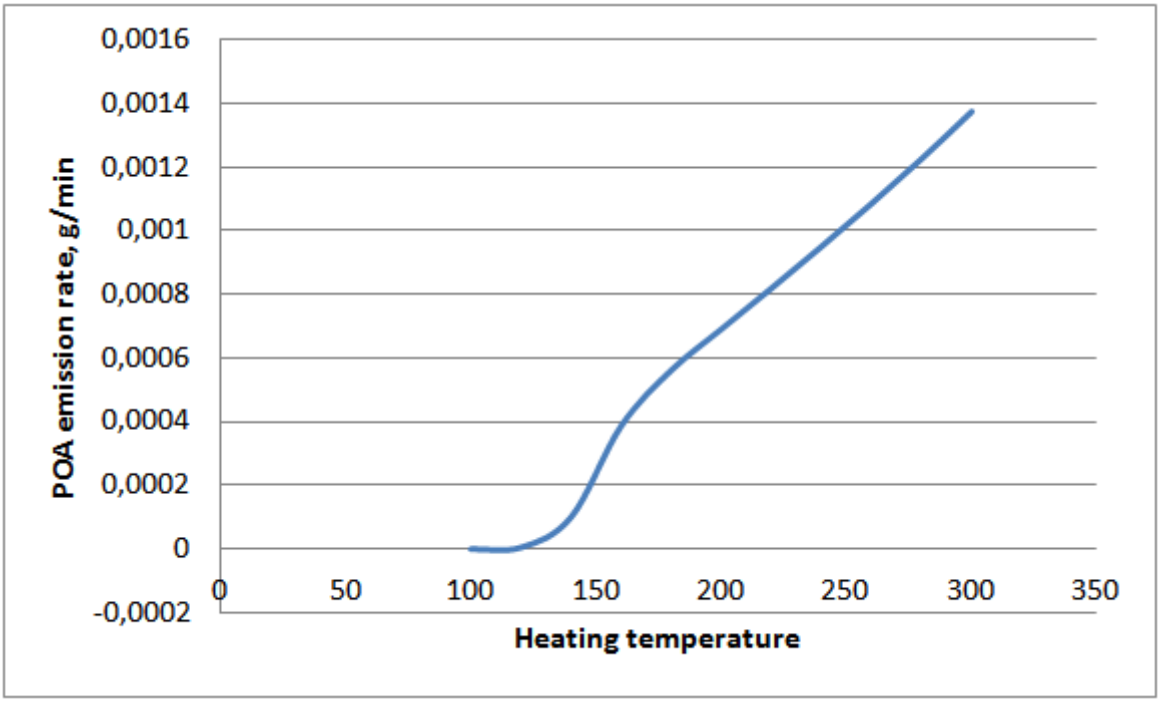

Figure 4-3: POA emission rate variation with corn oil temperature

The POA emission rate increased most when temperature of corn oil was increased from 100 °C to 120 °C. Further increase of temperature resulted in larger POA emission rates but less increment factor. The increment factor was defined as the ratio of POA emission rate at the temperature T_i and T_{i-1}.When heating temperature was set to 180 °C and higher, the increment factor changed slightly and became almost constant. This could be attributed to reaching smoke

point of simulated corn oil, above which the rate of VOC emission is almost the same (approximately 0.19 g/min).

Table 4-6: POA emission rate and its increment factor at different heating temperatures

Oil temperature, °C	POA, g/min	Increment factor
100	2.3189×10^{-7}	
120	5.46772×10^{-6}	23.5789383
140	0.000100732	18.42305202
160	0.000387768	3.849499003
180	0.000562977	1.451840621
200	0.000692222	1.229572481
220	0.000820927	1.185931303
240	0.000952177	1.159879979
260	0.001087275	1.141883169
280	0.001228057	1.129481487
300	0.001376489	1.120867416

Noteworthy, at temperatures below 180 °C no thermal alteration products including non-polar TG dimers, oxidized TG monomers and dimers were produced. This is in agreement with the experimental data [22], where the aforementioned thermal alteration products were obtained from frying vegetable oils at temperatures above 180 °C. The presence of oxidation products at relatively lower temperatures (100-160 °C) including VOCs can be explained by the autooxidation of oil, that take place due to the presence of oxygen in air at any temperature [53]. In other words, thermal oxidation reactions take place at 180 °C and higher, and below these values autooxidation of oil occurs.

It should be emphasized that due the compositions of COAs produced from corn oil heated to different temperatures vary as the equilibrium constant is a function of the temperature. As Table 4-7 presents, increasing the heating

temperature from 180 °C to 240 °C, led to the increase in the mass fractions of acrolein, palmitic and stearic acids. This increase could imply that there is more smoke produced above the pan at 240 °C compared to 180 °C, as these compounds are related to smoking. The oleic acid was observed in COA produced from heated oils at 180 °C, but it did not appear in COA at 240 °C. This shows that the rate of oxidation reactions involving unsaturated fatty acids increases with temperature. Expectedly, the mass fraction of glycerol in PM decreased with temperature, as it decomposed to produce acrolein. Additionally, the mass fraction of light aldehydes increased with heating temperature, since scission is favored at higher temperatures.

Table 4-7: The compositions of POA at different heating temperatures

Components	180 °C	240°C
Acrolein	6.35×10^{-8}	1.72×10^{-5}
Palmitic acid	1.95×10^{-7}	6.00×10^{-6}
Stearic acid	9.77×10^{-7}	2.82×10^{-5}
Oleic acid	4.02×10^{-8}	0
Glycerol	1.08×10^{-7}	5.59×10^{-9}
Octanal	1.94×10^{-11}	1.36×10^{-11}
Octanol	4.22×10^{-9}	1.86×10^{-9}
Heptanol	1.14×10^{-7}	5.62×10^{-8}
Nonene	0	6.23×10^{-13}
Octane	5.09×10^{-9}	1.73×10^{-9}
Heptane	1.71×10^{-8}	7.76×10^{-9}
Hexanal	4.02×10^{-8}	4.17×10^{-8}
Pentane	5.17×10^{-6}	3.50×10^{-6}
Pentanal	8.31×10^{-7}	1.01×10^{-6}
Methyl hydroxy heptanoate	5.74×10^{-7}	0
Methyl hydroxy octanoate	3.93×10^{-8}	0
Methyl oxo-nonananoate	5.88×10^{-9}	0
Methyl heptanoate	2.12×10^{-4}	2.88×10^{-8}
Methyl octanoate	2.75×10^{-3}	1.19×10^{-7}
Methyl nonenoate	1.37×10^{-7}	0
Methyl-8-oxooctanoate	5.69×10^{-8}	0
Heptanal	1.18×10^{-10}	1.60×10^{-10}

Methyl oxo-nonanoate	5.91×10^{-9}	0
Dimethyl Octanedioate	1.69×10^{-3}	0
Dimethyl Nonanedioate	3.10×10^{-4}	0
Ethanal	7.89×10^{-2}	0.108
Propanal	2.32×10^{-4}	4.94×10^{-4}
Butanal	2.47×10^{-5}	3.79×10^{-5}
Toluene	6.94×10^{-6}	1.72×10^{-6}
Cycloheptadiene	0.916	0.891

4.05 Effect of additives

POA mass emission rate during frying corn oil at 240 °C was 0.924 mg/min, while addition of myrcia increased the POA emission rate to 2.29 mg/min. The estimated increase in the POA emission rate is 2.5, which is higher than the increase in the experimental observations provided by Liu et al. [2]. To estimate the COA emission rate from stir-frying myrcia the equation 3.8 provided in the Methodology section was applied. The POA concentration from stir-frying myrcia reported by Liu et al. was 71 $\mu g/m^3$ and POA emission rate from 2 g of myrcia is equivalent to 0.001562 g/min. That is, the POA emission from stir-frying the condiment is 1.7 times greater than frying pure corn oil. The difference in the increment factor could be caused by the evaporation of VOCs during sampling that could lead to the underestimation of COA emissions [13]. Alternately, it was already mentioned that lack of tocopherols in the corn oil input could lead to increased rate of oxidation reactions. As a result, higher amount of VOCs from stir-frying myrcia in corn oil could be produced as shown by the simulation.

The composition of VOCs emitted from stir-frying myrcia is presented in Table 4-8. Similar to emission from heating corn oil at 240 °C, ethanal, pentane,

cycloheptadiene, propanal, toluene, butanal and acrolein were major VOCs emitted from stir-frying myrcia. Moreover, the cooking emissions from the condiment were enriched with methylpyrrole, heptane and terpenes. The abundance of terpenes, terpenoids and sesquiterpenes is attributed to the composition of the spice given in Table 3-4. The present model and the experiment published by Liu et al. [2] have different compounds dominating among the produced volatile products. To be more precise, in the experimental study methylpyrrole, monoterpenes and terpenoids had stronger signal intensity than other compounds. It should be emphasized that the molecular weight of terpenes, monoterpenes, and sesquiterpenes are less than the molecular weight of triglycerides and fatty acids. Therefore, in the experimental study the concentration of terpenes in vapor phase at the moment of fumes collection could be higher than oil products as they are more volatile. Moreover, as illustrated in Figure 2-2: The kinetic curve of polyunsaturated fatty acids oxidation Figure 2-2, oil oxidation products vary with time, and when the fumes were collected, the concentration of volatile products produced from oil alteration, caused by high temperature and air, could be low.

Table 4-8: The composition of VOCs emitted from stir-frying myrcia

Components	Mass fraction	Components	Mass fraction
Ethanal	0.55187853	Terpinen-4-ol	1.03×10^{-9}
Pentane	0.27068055	Glycerol	8.91×10^{-11}
Cycloheptadiene	0.1473284	Nonanal	5.97×10^{-11}
Propanal	0.01931534	Pyrrole	4.62×10^{-11}
Toluene	0.00219961	Methylpyridine	4.61×10^{-11}
Methylpyrrole	0.00057412	Pyrizine	3.00×10^{-11}
Butanal	0.0005663	Decene	1.95×10^{-11}
Heptane	0.00055697	g-terpene	1.13×10^{-11}
Acrolein	0.00035126	Terpinolene	1.09×10^{-11}
a-pinene	4.09×10^{-5}	Dimethyl Octanedioate	9.48×10^{-12}
Pentanal	2.95×10^{-5}	Methyl-8-Oxooctanoate	6.37×10^{-12}
Octane	2.94×10^{-5}	Decanal	3.64×10^{-12}
Cyclopentene	1.40×10^{-5}	Methyl Heptanoate	3.28×10^{-12}
b-pinene	1.38×10^{-5}	Pentadienal	1.19×10^{-12}
Carvone	2.58×10^{-6}	Pyrrolidine	1.14×10^{-12}
Spathulenol	2.41×10^{-6}	Nonenal	1.04×10^{-12}
Hexanal	1.98×10^{-6}	Dimethyl nonanedioate	4.30×10^{-13}
a-campholenal	1.71×10^{-6}	Methyl-oxononanoate	2.91×10^{-13}
p-cymene	1.39×10^{-6}	Methylhydroxyoctanoate	1.36×10^{-13}
2-butenal	8.54×10^{-7}	Decenal	4.44×10^{-14}
Methyl heptanoate	7.34×10^{-7}	Nonadiene	4.28×10^{-14}
Isoprene	7.33×10^{-7}	B-Caryophyllene	2.48×10^{-14}
1.3-pentadiene	3.50×10^{-7}	Methyloxodecanoate	1.32×10^{-14}
a-humulene	2.21×10^{-7}	Calamene	8.27×10^{-15}
Furan	5.48×10^{-8}	Myrcene	7.37×10^{-15}
p-methylacetophenone	5.41×10^{-8}	Methyl Nonenoate	5.68×10^{-15}
Heptenal	5.29×10^{-8}	A-Calacorene	5.03×10^{-15}
Heptanal	1.32×10^{-8}	Limonene	3.95×10^{-15}
p-cymenene	3.38×10^{-9}	Undecadienal	1.48×10^{-15}
Octanol	2.43×10^{-9}	D-Cadinene	9.82×10^{-16}
Methyl octanoate	2.11×10^{-9}	Palmitic acid	3.04×10^{-17}
Octanal	1.41×10^{-9}	Oleic acid	1.28×10^{-17}
Nonene	1.10×10^{-9}		

Similar to experimental data, the emission of aldehydes from stir-frying

myrcia largely enhanced compared with those from heating pure corn oil. The enhancement factor increases with carbon number, such that lighter aldehydes were enhanced less than heavier one.

Table 4-9: The enhancement factors and mass fraction of aldehydes in VOCs from heating corn oil and stir-frying myrcia.

Components	Myrcia	Corn	Enhancement factor
Ethanal	0.55188	0.22335	2.47091
Propanal	0.01932	0.00668	2.89152
Butanal	0.00057	0.00017	3.33118
Pentanal	2.95×10^{-5}	6.11×10^{-6}	4.82815
Hexanal	1.98×10^{-6}	3.37×10^{-7}	5.87537
Heptanal	1.32×10^{-8}	1.83×10^{-9}	7.21311
Octanal	1.41×10^{-9}	1.56×10^{-10}	9.03846
Nonanal	5.97×10^{-11}	5.20×10^{-12}	11.4808
Decanal	3.64×10^{-12}	2.46×10^{-13}	14.7967

As Table 4-9 shows, there is almost a linear increase of enhancement factor with number of carbons in aldehydes. Mass fractions of octanal, nonanal, and decanal have increased by an order of magnitude, because they are present in myrcia oil subjected to frying.

It should be emphasized that total PM emission rate increased with addition of myrcia as well. As it was already mentioned, the total PM from heating corn, soybean and sunflower oils was dominated by water that contributed to 99%, 97% and 96% of total PM, respectively. In case of stir-frying myrcia, this value has dropped to 72% leading to 1.5 times more PM mass emitted compared to those emitted from heating oils at 240 °C. This observation could be interpreted as higher interaction between oil and spice

components than that between oil and water molecules. When myrcia was added, the tendency of water to appear in liquid phase decreased as can be seen in Table 4-3 and Table 4-10, such that K value of water in emissions from cooking oils was approximately 0.012 and it increased to 0.013. This change could be related to the introduction of more volatile components to the cooking fumes from stir-frying myrcia that have a lower K value than water. Comparing K values of components presented in Table 4-3 and Table 4-10, it is seen that number of organic compounds with K value less than 1 increased. That is, the contribution of organics to PM has increased. The correlation between K values of water and its contribution to PM mass emission rate shows that the composition of the PM can be predicted by estimating the tendency of the component to appear in vapor phase relative to particulate phase.

Simulation results demonstrated that further addition of myrcia to corn oil further increased COA emissions while decreasing contribution of water molecules to PM as illustrated in Figure 4-4. A linear relation between the mass of the condiment added and COA emission rate was noted. Reductions in the water content in total PM supports the notion of strong interaction between myrcia and oil components that reinforce with addition of a seasoning.

Table 4-10: K values from compounds found in PM from stir-frying myrcia

Components	K values	Components	K values
Oxygen	765.002	Dimethyl nonanedioate	1.29×10^{-5}
Nitrogen	1112.964	Ethanal	1.724827
Water	0.013312	Propanal	2.157375
Acrolein	1.443255	Butanal	0.552197
Glycerol	2.34×10^{-8}	Methylpyrrole	0.012372
Nonanal	0.00897	Pentadienal	0.038632
Octanal	0.043636	Toluene	1.415528
Decanal	0.000442	Cycloheptadiene	0.022218
Octanol	0.000363	a-pinene	0.002222
Heptenal	0.001644	b-pinene	0.001454
Decene	0.004622	p-cymene	0.037169
Nonene	0.020022	g-terpene	0.00049
Octane	0.484049	Terpinolene	0.0004
Heptane	1.640512	p-cymenene	0.000432
Hexanal	0.497521	a-campholenal	0.000176
Pentane	34.0618	Terpinen-4-ol	4.74×10^{-6}
Nonenal	0.006499	p-methylacetophenone	3.59×10^{-5}
Pentanal	0.977743	Carvone	4.12×10^{-5}
Methyl Heptanoate	1.44×10^{-5}	a-humulene	6.49×10^{-6}
Methylhydroxyoctanoate	3.9×10^{-6}	Spathulenol	3.42×10^{-8}
Methyl-Oxononanoate	7.83×10^{-5}	Pyrrole	0.004153
Methyl heptanoate	0.006903	Furan	0.443195
Methyl octanoate	0.00016	Isoprene	43.94132
Methyl-8-Oxooctanoate	0.000299	Cyclopentene	25.55312
Heptanal	0.205928	2-butenal	0.03589
Methyl-Oxononanoate	7.83×10^{-5}	Pyrrolidine	0.043351
Dimethyl Octanedioate	5.27×10^{-5}	Pyrazine	0.011653
Methylpyridine	0.037872	Pentadienal	0.276291

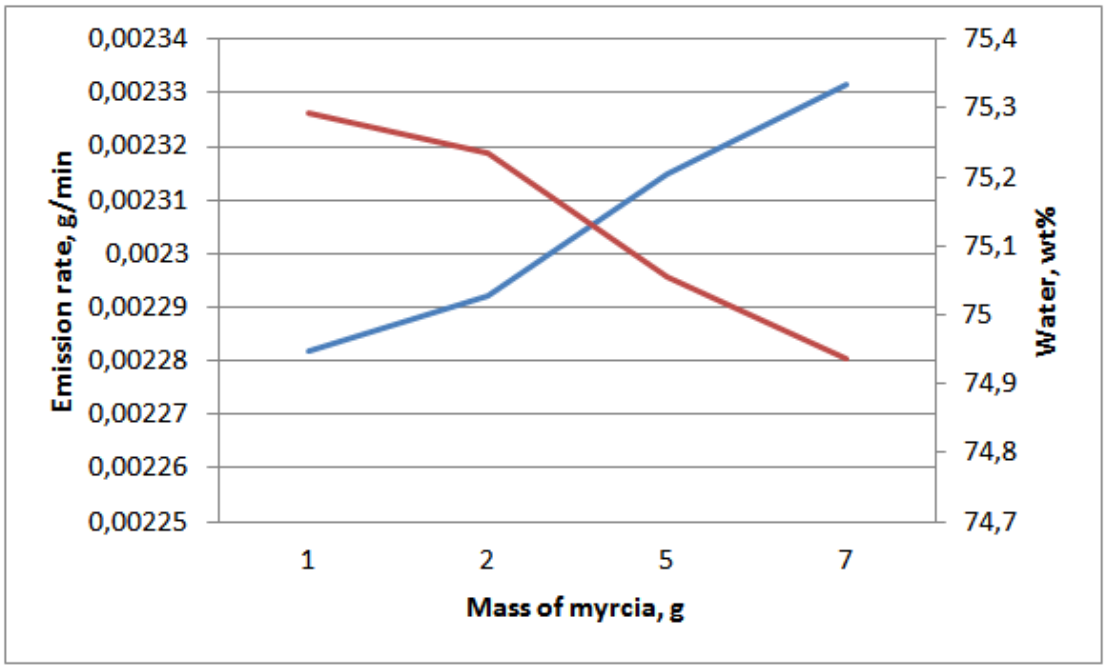

Figure 4-4: Variation of POA emission rate and contribution of water to PM with mass of myrcia

The simulation results show that POA emission rates from corn, soybean and sunflower oils vary listed in ascending order, due to the difference in the unsaturated free fatty acids compositions. The compositions of VOCs emitted from heated soybean and sunflower oils comprised wider groups of compounds resulting in higher contribution to COA. While temperatures of the reactors were increased, an increase in the VOC emission rate and, consequently, COA formation rate was observed. Opposite effect was observed while the temperature of the indoor air was increased, since the supersaturation of the vapor mixture was not observed below one until the temperature decreased to 36 °C. COA emission rate increased with addition of myrcia, since VOCs from stir-frying myrcia contained more organic compounds that partitioned into

particulate phase. The composition of COAs varied with the change of indoor air temperature and heating temperature.

Chapter 5- Conclusions

In summary, using the vegetable oils with higher unsaturated free fatty acid composition oils in the absence of other cooking ingredients produces higher rates of COA. This increase was attributed to the higher rates of oxidation reactions yielding VOCs that partitioned into particulate phase. It was found that the composition and emission rate of COA vary with heating temperature. Short chain hydrocarbons were favored at higher temperatures. Additionally, increase in the ambient temperature results in the reduction of COA emission rate, as the saturation ratio of the VOCs decreased. Moreover, the aerosol water absorption rate decreased with indoor air temperature. There is also evidence of significant increase in the COA emission rate and drastic change in the COA composition with addition of myrcia.

This thesis work shows that the computer simulations can be used to predict the indoor cooking aerosol formation for complex and dynamic systems where phase and chemical equilibria coexist. Although this study made a reliable contribution to understanding cooking as a source of indoor air pollutants, the efficiency of antioxidants on decreasing the tendency of oil to oxidize was not studied. Moreover, this study did not consider higher order

triglyceride polymers that could result in the overestimation of vapors produced from heated cooking oils.

Therefore, it is recommended to incorporate tocopherols in the vegetable oil composition. Moreover, more oxidized and non-oxidized oligomers could be introduced as a product of thermal alteration and oxidation products. Moreover, The current simulation can be extended to simulate the cooking process with other cooking additives if sufficient experimental information on the composition of ingredients and VOCs is available. Although several assumptions were made to simplify the frying operation, it can be further improved using future empirical data. Moreover, the current model can further be evolved to consider the contribution of cooking operations to secondary organic aerosol (SOA) by incorporating a reactor, where ozonolysis of the terpenes found in myrcia would be simulated. Additionally, the effect of the relative humidity on the COA formation can be studied.

Reference List

1. WHO. WHO | Household air pollution and health [Internet]. WHO media centre. 2014. Available from: http://www.who.int/mediacentre/factsheets/fs292/en/
2. Liu T, Liu Q, Li Z, Huo L, Chan MN, Li X, et al. Emission of volatile organic compounds and production of secondary organic aerosol from stir-frying spices. Sci Total Environ [Internet]. Elsevier B.V.; 2017;599–600:1614–21. Available from: http://dx.doi.org/10.1016/j.scitotenv.2017.05.147
3. Mohr C, Huffman JA, Cubison MJ, Aiken AC, Docherty KS, Kimmel JR, et al. Characterization of primary organic aerosol emissions from meat cooking, trash burning, and motor vehicles with high-resolution aerosol mass spectrometry and comparison with ambient and chamber observations. Environ Sci Technol. 2009;43(7):2443–9.
4. Allan JD, Williams PI, Morgan WT, Martin CL, Flynn MJ, Lee J, et al. Contributions from transport, solid fuel burning and cooking to primary organic aerosols in two UK cities. Atmos Chem Phys [Internet]. 2010;10(2):647–68. Available from: http://www.atmos-chem-phys.net/10/647/2010/
5. Crippa M, Canonaco F, Slowik JG, El Haddad I, Decarlo PF, Mohr C, et al. Primary and secondary organic aerosol origin by combined gas-particle phase source apportionment. Atmos Chem Phys. 2013;13(16):8411–26.
6. Abdullahi KL, Delgado-Saborit JM, Harrison RM. Emissions and indoor concentrations of particulate matter and its specific chemical components from cooking: A review. Atmos Environ [Internet]. Elsevier Ltd; 2013;71:260–94. Available from: http://dx.doi.org/10.1016/j.atmosenv.2013.01.061
7. Kaltsonoudis C, Kostenidou E, Louvaris E, Psichoudaki M, Tsiligiannis E, Florou K, et

al. Characterization of fresh and aged organic aerosol emissions from meat charbroiling. Atmos Chem Phys. 2017;17(11):7143–55.

8. Amouei Torkmahalleh M, Gorjinezhad S, Unluevcek HS, Hopke PK. Review of factors impacting emission/concentration of cooking generated particulate matter. Sci Total Environ [Internet]. Elsevier B.V.; 2017;586:1046–56. Available from: http://dx.doi.org/10.1016/j.scitotenv.2017.02.088
9. Torkmahalleh MA, Goldasteh I, Zhao Y, Udochu NM, Rossner A, Hopke PK, et al. PM 2.5 and ultrafine particles emitted during heating of commercial cooking oils. Indoor Air. 2012;22(6):483–91.
10. Amouei Torkmahalleh M, Zhao Y, Hopke PK, Rossner A, Ferro AR. Additive impacts on particle emissions from heating low emitting cooking oils. Atmos Environ. 2013;74:194–8.
11. Klein F, Farren NJ, Bozzetti C, Daellenbach KR, Kilic D, Kumar NK, et al. Indoor terpene emissions from cooking with herbs and pepper and their secondary organic aerosol production potential. Sci Rep. 2016;6(April):1–2.
12. Hallquist M, Wenger JC, Baltensperger U, Rudich Y, Simpson D, Claeys M, et al. The formation, properties and impact of secondary organic aerosol: current and emerging issues. Atmos Chem Phys [Internet]. 2009;9(14):5155–236. Available from: http://www.atmos-chem-phys.net/9/5155/2009/%5Cnhttp://www.atmos-chem-phys.net/9/5155/2009/acp-9-5155-2009.pdf
13. Torkmahalleh MA, Kaibaldiyeva U, Kadyrbayeva A. A new computer model for the simulation of particulate matter formation from heated cooking oils using Aspen Plus. Build Simul. 2017;10(4):535–50.
14. World Health Organization. Health Effects of Particulate Matter: Policy implications for countries in eastern Europe, Caucasus and central Asia. J Korean Med Assoc

[Internet]. 2013;50(2):20. Available from: http://synapse.koreamed.org/DOIx.php?id=10.5124/jkma.2007.50.2.175

15. McMurry P, Shepherd M, Vickery J. Particulate Matter Science for Policy Makers: A NARSTO Assessment; Chapter 3: Atmospheric Aerosol Processes. 2004; Available from: https://application.wiley-vch.de/books/sample/3527336451_c01.pdf
16. Dobarganes MC. Formation of New Compounds during Frying - General Observations [Internet]. AOCS Lipid Library. 2018. Available from: https://ediblesciencefaire.wordpress.com/2011/06/01/maillard-reaction/
17. Shahidi F. Bailey ' S Industrial Oil and Fat. Vol. 1, Wiley interscience. 2009. 2005-2006 p.
18. Air I, Nahrungsmittel PB. VENTILATION IN KITCHEN – AEROSOL CONCENTRATION AND KEY COMPONENTS IN THE VAPOUR. 2002;292–7.
19. Denisov ET, Afanas'ev IB. Oxidation and Antioxidants in Organic Chemistry and Biology. Food Lipids: Chemistry, Nutrition, and Biotechnology. 2008. 299-320 p.
20. Sebedlo J-L, Juaneda P. Isomeric and Cyclic Fatty Acids as a Result of Frying. In: Erickson MD, editor. Deep frying: chemistry, nutrition, and practical applications. 2nd ed. 2007. p. 57–86.
21. Scrimgeour C. Chemistry of Fatty Acids. In: Shahidi F, editor. BAILEY'S INDUSTRIAL OIL AND FAT PRODUCTS. 6, volume ed. A John Wiley & Sons, Inc.; 2005. p. 1–44.
22. Dobarganes MC, Márquez-Ruiz G. Formation and Analysis of Oxidized Monomeric, Dimeric, and Higher Oligomeric Triglycerides. In: Erickson MD, editor. Deep Frying: Chemistry, Nutrition, and Practical Applications: Second Edition. 2nd ed. 2007. p. 87–110.
23. Perkins EG. Volatile Odor and Flavor Components Formed in Deep Frying. In:

Ericson, Michael D, editor. Deep frying:chemistry, nutrition, and practical applications. 2nd ed. 2007. p. 51–6.

24. Gurr MI, Harwood JL, Frayn KN, editors. Lipids: definition, isolation, separation and detection. In: LIpid biochemistry. 5th ed. Blackwell Science; 2002. p. 1–12.

25. Schaich KM. Lipid Oxidation: Theoretical Aspects. In: Shahidi F, editor. BAILEY'S INDUSTRIAL OIL AND FAT PRODUCTS. 6th ed. A John Wiley & Sons, Inc.; 2005. p. 219–357.

26. Gunstone F., Knothe G, Kenar JA. Chemical Properties. In: Gunstone FG, Harwood JL, Dijkstra AJ, editors. The Lipid Handbook. 3rd ed. Boca Raton: Taylor & Francis Group; 2007. p. 535–89.

27. Denisov ET, Afanas'ev IB, editors. Molecular Products and Thermochemistry of Hydrocarbon Oxidation. In: Oxidation and Antioxidants in Organic Chemistry and Biology. Taylor & Francis Group; 2005. p. 1–18.

28. Kamal-Eldina A, Mäkinenb M, Lampib A-M. The Challenging Contribution of Hydroperoxides to the Lipid Oxidation Mechanism. In: Kamal-Eldin A, editor. Lipid Oxidation Pathways. AOCS Press; 2003. p. 1–36.

29. Christie WW, Dobson G. Formation of cyclic fatty acids during. Vol. 102. 2000. p. 515–20.

30. Aspen Technology Inc. Thermodynamic property models. Aspen Phys Prop Syst - Phys Prop Model. 2010;12–184.

31. E.H. Pechan & Associates Inc. Documentation for the final 2002 nonpoint sector national emission inventory for criteria and hazardous air pollutants. Reports. Durham; 2005.

32. Ots R, Vieno M, Allan JD, Reis S, Nemitz E, Young DE, et al. Model simulations of cooking organic aerosol (COA) over the UK using estimates of emissions based on

measurements at two sites in London. Atmos Chem Phys. 2016;16(21):13773–89.

33. Yenumala SR, Maity SK. Reforming of vegetable oil for production of hydrogen: A thermodynamic analysis. J Hydrog Energy. 2011;36(18):11666–75.

34. Bridgeman OC., Aldrich EW. Vapor pressure tables for water. J Heat Transf. 1964;(86):279–86.

35. Warner K. Chemistry of Frying Oils. In: Food lipids: chemistry, nutrition, and biotechnology. Illinois: Marcel Dekker, Inc; 2002. p. 223–40.

36. Gloria M-R. Analysis of Used Frying Oils and Fats by High-Performance Size-Exclusion Chromatography - AOCS Lipid Library. 2018.

37. Vo U-U t., Morris MP. Non-volatile, Seni-volatile, or Volatile : Redefining Volatile for Volatile Organic Compounds. South Coast Air Qual Manag Dist. 2012;4182(December):1–19.

38. Aspen Technology Inc. Aspen Physical Property System. Engineering. 2001. 1-436 p.

39. Zoghbi MGB, Andrade EHA, da Silva MHL, Carreira LMM, Maia JGS. Essential oils from three Myrcia species. Flavour Fragr J. 2003;18(5):421–4.

40. Parthasarathy VA, Chempakam B, Zachariah TJ. Chemistry of Spices. Parthasarathy VA, Chempakam B, Zachariah TJ, editors. Pondicherry, India: Biddles Ltd, King's Lynn.; 2008.

41. Gmehling J, Kolbe B, Kleiber M, Rarey J. No TitleChemical Thermodynamics for Process Simulation. Weinheim, Germany: Wiley-VCH; 2012.

42. Gretscher H, Schaber K. Aerosol formation by heterogeneous nucleation in wet scrubbing. Chem Eng Process Process Intensif. 1999;38(4–6):541–8.

43. McMurry PH, Fink M, Sakurai H, Stolzenburg MR, Mauldin IL, Smith J, et al. A criterion for new particle formation in the sulfur-rich Atlanta atmosphere. J Geophys Res Atmos. 2005;110(22):1–10.

44. Mühlberger F, Wieser J, Ulrich A, Zimmermann R. Single photonIonization, Mass, (SPI) via incoherent VUV-excimer light: robust and compact time-of-flight spectrometer for on-line, real-time process gas analysis. Anal Chem. 2002;74:3790–3801.

45. Mühlberger, F., Hafner, K., Kaesdorf, S., Ferge, T., Zimmermann R. Comprehensive Resonance enhanced multiphoton, on-line characterization of complex gas mixtures by quasi-simultaneous ionization, vacuum-UV single-photon ionization, and electron Characterization., impact ionization in a time-of-flight mass spectrometer: s. Anal Chem. 2004;76:6753–6764.

46. Fullana A, Carbonell-Barrachina AA, Sidhu S. Comparison of volatile aldehydes present in cooking fumes of extra virgin olive, olive, and canola oils. J Agric Food Chem. 2004;52:5207–14.

47. Klein F, Platt SM, Farren NJ, Detournay A, Bruns EA, Bozzetti C, et al. Characterization of gas-phase organics using proton transfer reaction time-of-flight mass spectrometry: cooking emissions. Environ Sci Technol. 2016;50:1243–1250.

48. Katragadda, H.R., Fullana, A., Sidhu, S., Carbonell-Barrachina ÁA. Emissions of volatile aldehydes from heated cooking oils. Food Chem. 2010;120:59–65.

49. Hwang LS. Sesame oil. In: Bailey's industrial oil and fat products. John Wiley & Sons; 2005. p. 537–77.

50. Shahidi F, Zhong Y. Antioxidants: Regulatory Status. In: Shahidi F, editor. BAILEY'S INDUSTRIAL OIL AND FAT PRODUCTS. 6th ed. John Wiley & Sons, Inc.; 2005. p. 491–510.

51. Khlystov A, Stanier CO, Takahama S, Pandis SN. Water content of ambient aerosol during the Pittsburgh air quality study. J Geophys Res Atmos. 2005;110(7):1–10.

52. Ansari AS, Pandis SN. Water absorption by secondary organic aerosol and its effect on

inorganic aerosol behavior. Vol. 34, Environmental Science and Technology. 2000. p. 71–7.

53. Choe E, Min DB. Comprehensive Reviews in Food Science and Food Safety Mechanisms and Factors for Edible Oil Oxidation. Compr Rev Food Sci Food Saf. 2006;5:169–86.

54. CheGuide. Joback method [Internet]. 2018. Available from: https://cheguide.com/tag/joback-method/

Appendices

Appendix A

In this section, scission of unsaturated acids during oxidation is illustrated.

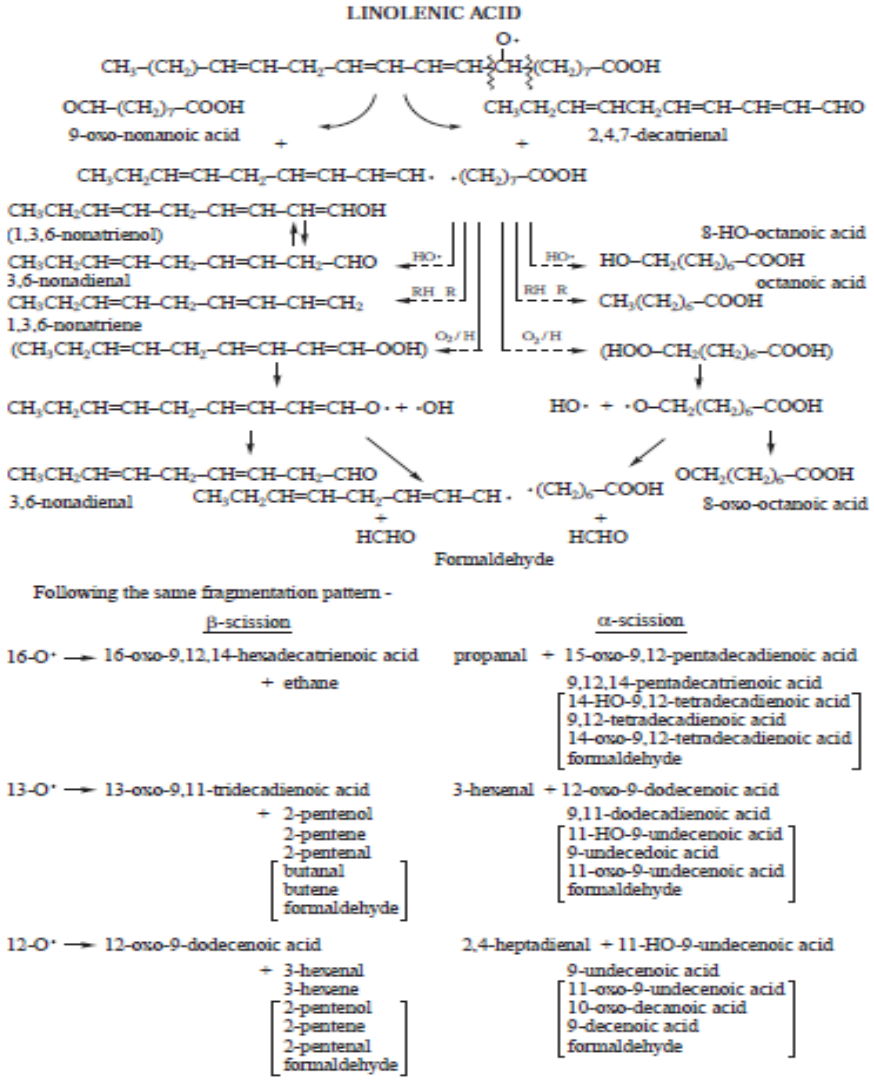

Figure A-1: Oxidation routes for linolenic acid[50]

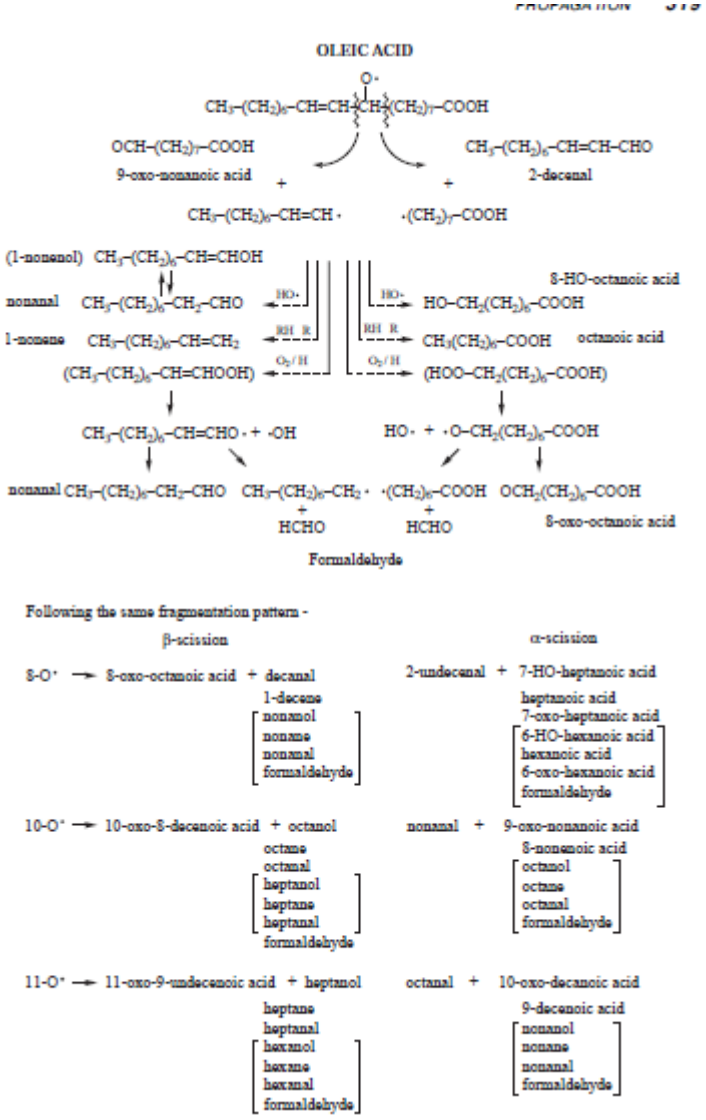

Figure A-2: Oxidation routes for oleic acid [50]

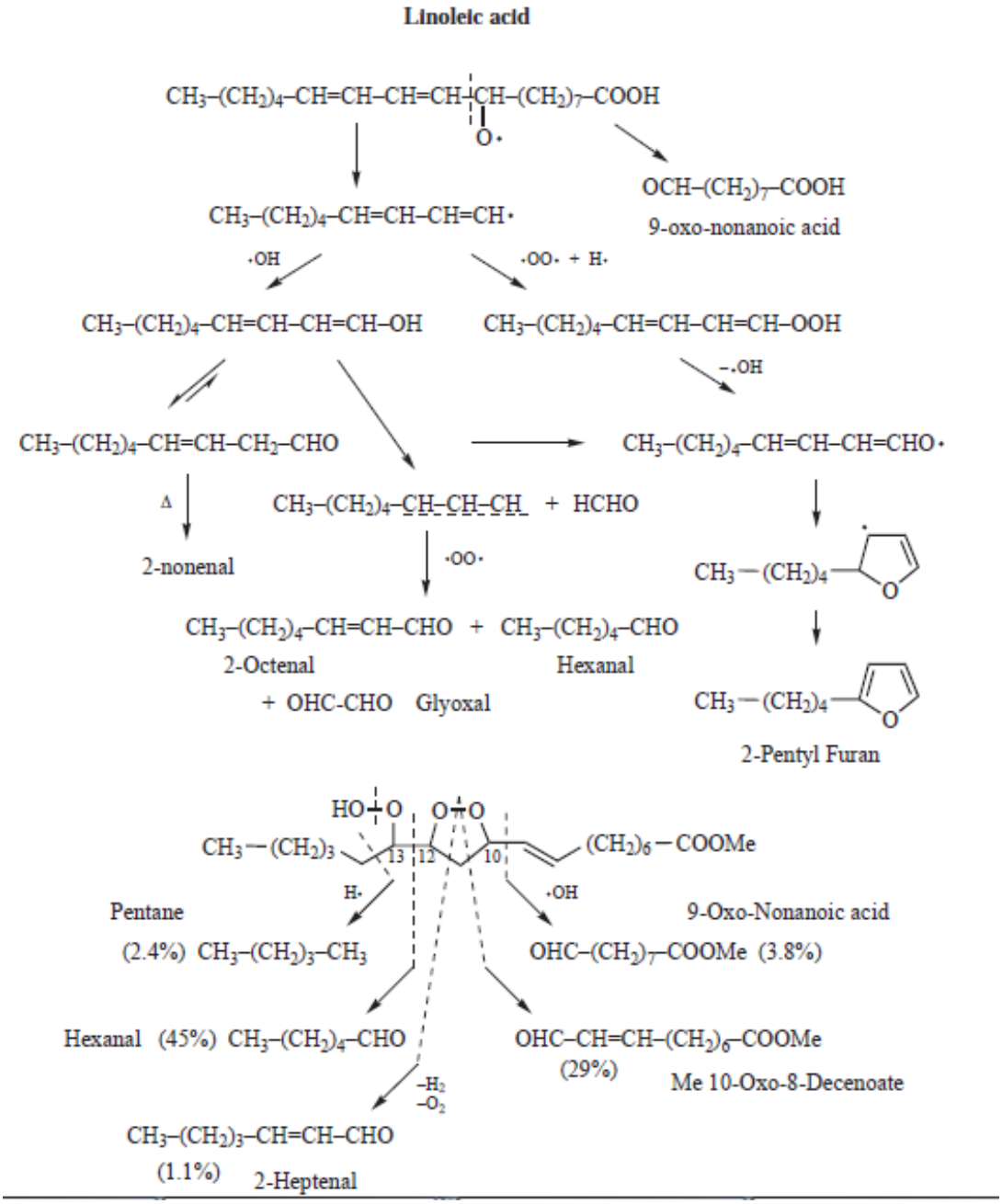

Figure A-3: Oxidation routes for linoleic acid[50]

Appendix B

Table B-1: Non-volatile components included in the simulation

Oxidized triglyceride monomers
Oxidized triolein with epoxyoleic acid
Oxidized trilinolein with epoxylinoleic acid at carbons 9,10
Oxidized trilinolein with epoxylinoleic acid at carbons 12,13
Oxidized triolein with hydroperoxy acid at carbon 8
Oxidized triolein with hydroperoxy acid at carbon 9
Oxidized triolein with hydroperoxy acid at carbon 10
Oxidized triolein with hydroperoxy acid at carbon 11
Oxidized triolein with cis-9, trans-11,13-hydroxy-octadecanoic acid
Oxidized triolein with trans-10, trans-12, 9-hydroxy-octadecanoic acid
Oxidized triolein with keto acid at carbon 8
Oxidized triolein with keto acid at carbon 9
Oxidized triolein with keto acid at carbon 10
Oxidized triolein with keto acid at carbon 11
Oxidized triolein with cis-9, trans-11,13-keto-octadecanoic acid
Oxidized triolein with trans-10, trans-12, 9-keto-octadecanoic acid
Cyclized triglyceride monomers
Trilinolenin with cyclohexene between carbons 10,15
Trilinolenin with cyclohexene between carbons 10,15
Trilinolenin with cyclopentene between carbons 11,15
Trilinolenin with cyclopentene between carbons 10,14
Trilinolein with cyclopentene between carbons 10,14
Trilinolein with cyclopentene between carbons 10,15
Trilinolein with cyclopentene between carbons 8,2
Trilinolein with cyclopentene between carbons 8,3
Trilinolein with cyclohexane between carbons 5,10
Trilinolein with cyclopentane between carbons 13,17
Trilinolein with cyclopentane between carbons 5,9
Trilinolein with cyclohexane between carbons 12,17
Trilinolein with bicyclic group between carbons 10,15
Trilinolein with bicyclic group between carbons 10,14
Triolein with cyclohexane between carbons 4,9
Triolein with cyclopentane between carbons 5,9
Triolein with cyclopentane between carbons 10,14
Triolein with bicyclic group between carbons 10,15
Non-polar dimers
Nonpolar dimer of triolein at carbon 8
Nonpolar dimer of triolein at carbon 11
Nonpolar dimer of trilinolein at carbon 5

Nonpolar dimer of trilinolein at carbon 8
Nonpolar dimer of trilinolein at carbon 11
Nonpolar dimer of trilinolenin at carbon 2
Nonpolar dimer of trilinolenin at carbon 5
Nonpolar dimer of trilinolenin at carbon 8
Nonpolar dimer of trilinolenin at carbon 11
Acyclic dimer with C-O-C linkage
Odixized triolein dimer with oxygen at carbon 8
Odixized triolein dimer with oxygen at carbon 11
Odixized trilinolein dimer with oxygen at carbon 5
Odixized trilinolein dimer with oxygen at carbon 8
Odixized trilinolein dimer with oxygen at carbon 11
Odixized trilinolenin dimer with oxygen at carbon 2
Odixized trilinolenin dimer with oxygen at carbon 5
Odixized trilinolenin dimer with oxygen at carbon 8
Odixized trilinolenin dimer with oxygen at carbon 11
Oxidized triglyceride with monohydroxy, dihydroxy, keto groups
Oxidized triolein dimer with 8-hydroxy octadecenoic acid
Oxidized triolein dimer with 9-hydroxy octadecenoic acid
Oxidized triolein dimer with 10-hydroxy octadecenoic acid
Oxidized triolein dimer with 11-hydroxy octadecenoic acid
Oxidized trilinolein dimer with cis-9, trans-11,13-hydroxy-octadecanoic acid
Oxidized trilinolein dimer with trans-10, trans-12, 9-hydroxy-octadecanoic acid
Oxidized triolein dimer with two 8-hydroxy octadecenoic acid groups
Oxidized triolein dimer with two 9-hydroxy octadecenoic acid groups
Oxidized triolein dimer with two 10-hydroxy octadecenoic acid groups
Oxidized triolein dimer with two 11-hydroxy octadecenoic acid groups
Oxidized trilinolein dimer with two cis-9, trans-11,13-hydroxy-octadecanoic acid groups
Oxidized trilinolein dimer with two trans-10, trans-12, 9-hydroxy-octadecanoic acid groups
Oxidized triolein dimer with 8-keto octadecenoic acid
Oxidized triolein dimer with 9-keto octadecenoic acid
Oxidized triolein dimer with 10-keto octadecenoic acid
Oxidized triolein dimer with 11-keto octadecenoic acid
Oxidized trilinolein dimer with two cis-9, trans-11,13-keto-octadecanoic acid groups
Oxidized trilinolein dimer with two trans-10, trans-12, 9-keto-octadecanoic acid groups

Appendix C

Table C- 1: Standard enthalpy of formation for components required by Aspen Plus

Component	Method	Estimated H_f, kJ/mol	Component	Method	Estimated H_f, kJ/mol
Dilinolein	Benson	-1189,402	Odixized trilinolein dimer with oxygen at carbon 11	Gani	-3101,2
Dilinolenin	Benson	-961,902	Odixized trilinolenin dimer with oxygen at carbon 2	Gani	-2423,6
Diolein	Benson	-1416,902	Odixized trilinolenin dimer with oxygen at carbon 5	Gani	-2423,6
Monolinolein	Benson	-881,701	Odixized trilinolenin dimer with oxygen at carbon 8	Gani	-2423,6
Monolinolein	Benson	-767,951	Odixized trilinolenin dimer with oxygen at carbon 11	Gani	-2423,6
Monoolein	Benson	-995,451	Oxidized triolein with hydroperoxy acid at carbon 8	Joback	-3818,4
Monostearin	Benson	-1105,651	Oxidized triolein with hydroperoxy acid at carbon 9	Joback	-3957,9
Monopalmitin	Benson	-1065,791	Oxidized triolein with hydroperoxy acid at carbon 10	Joback	-3684,6
Methylhydroxyheptanoate	Benson	-663,781	Oxidized triolein with hydroperoxy acid at carbon 11	Joback	-3907,5
Methylhydroxyoctanoate	Benson	-683,711	Oxidized triolein with cis-9, trans-11,13-hydroxy-octadecanoic acid	Joback	-3204,2
Cyclic trilinolein with cyclopentene	Benson	-1560,513	Oxidized triolein with trans-10, trans-12, 9-hydroxy-octadecanoic acid	Joback	-3204,2
Cyclic trilinolein with cyclohexene	Benson	-1531,193	Oxidized trilinolein dimer with two cis-9, trans-11,13-hydroxy-octadecanoic acid groups	Joback	-3493,9
Methyl heptanoate	Benson	-513,391	Oxidized trilinolein dimer with two trans-10, trans-12, 9-hydroxy-octadecanoic acid groups	Joback	-3493,9
Nonpolar trilinolein dimer-carbon 2	Gani	-2965,166	Oxidized triolein dimer with two 8-hydroxy octadecenoic acid groups	Joback	-4197,2
Nonpolar trilinolein dimer-carbon 5	Gani	-2968,666	Oxidized triolein dimer with two 9-hydroxy octadecenoic acid groups	Joback	-4206,3
Nonpolar trilinolein dimer-carbon 8	Gani	-2968,666	Oxidized triolein dimer with two 10-hydroxy octadecenoic acid groups	Joback	-4206,3
Nonpolar trilinolenin dimer-carbon 2	Gani	-2282,666	Oxidized triolein dimer with two 11-hydroxy octadecenoic acid groups	Joback	-4197,2
Nonpolar trilinolenin dimer-carbon 5	Gani	-2286,166	Oxidized triolein dimer with 8-keto octadecenoic acid	Gani	-3752,5
Nonpolar trilinolenin dimer-carbon 8	Gani	-2282,666	Oxidized triolein dimer with 9-keto octadecenoic acid	Gani	-3752,5
Nonpolar trilinolenin dimer-carbon 11	Gani	-2282,666	Oxidized triolein dimer with 10-keto octadecenoic acid	Gani	-3752,5
Oxidized triolein dimer with oxygen at carbon 8	Gani	-3778,859	Oxidized triolein dimer with 11-keto octadecenoic acid	Gani	-3752,5
Oxidized triolein dimer with oxygen at carbon 11	Gani	-3778,859	Oxidized trilinolein dimer with two cis-9, trans-11,13-keto-octadecanoic acid groups	Gani	-3076,4
Odixized trilinolein dimer with oxygen at carbon 5	Gani	-3101,237	Oxidized trilinolein dimer with two trans-10, trans-12, 9-keto-octadecanoic acid groups	Gani	-3076,4
Odixized trilinolein dimer with oxygen at carbon 8	Gani	-3101,237			

C.1 Joback method

Joback method is a first-order group contribution method that estimates thermophysical properties of a component as a sum of group parameters [54].

To estimate the standard enthalpy of formation the following equation is used:

$$H_{formation} = 68.29 + \sum H_{form,i} \quad \text{(C.1)}$$

With $H_{formation}$ representing the standard enthalpy of formation in kJ/mol, and $\sum H_{form,i}$ is the sum of enthalpies of formation of i number of functional groups.

C.2 Gani method

$$H_f = 5.549 + \sum_i N_i H_{f1i} + \sum_j M_j H_{f2j} + \sum_k O_k H_{f3k} \quad \text{(C.2)}$$

Where N_i, M_j, and O_k is the first-, second-, and third-order groups.

C.3 Benson method

Benson's approach is based on the assumption that the properties of the larger molecules can be estimated by the as the sum of the contributions from the individual atoms or bonds in the molecule, therefore it is a second-order group contribution.

Appendix D

Table D--1: VOC composition (mass fraction) from frying oils

Components	Corn	Soybean	Sunflower
Acrolein	9,44 x10^{-5}	0,00034	0,00035
Palmitic acid	2,56 x10^{-8}	2,06 x10^{-11}	1,78 x10^{-11}
Stearic acid	1,07 x10^{-7}	8,40 x10^{-10}	8,89 x10^{-10}
Oleic acid	1,26 x10^{-19}	9,01 x10^{-18}	8,94 x10^{-18}
Glycerol	2,13 x10^{-11}	7,76 x10^{-11}	7,60 x10^{-11}
Undecanal	7,02 x10^{-17}	1,26 x10^{-15}	1,26 x10^{-15}
Decanadiene	6,94 x10^{-15}	4,00 x10^{-14}	4,01 x10^{-14}
Nonanal	5,20 x10^{-12}	5,03 x10^{-11}	4,98 x10^{-11}
Octanal	1,56 x10^{-10}	1,21 x10^{-9}	1,19 x10^{-9}
Decanal	2,46 x10^{-13}	3,01 x10^{-12}	2,98 x10^{-12}
Octanol	2,27 x10^{-10}	1,96 x10^{-9}	1,91 x10^{-9}
Heptenal	6,55 x10^{-9}	4,34 x10^{-8}	4,24 x10^{-8}
Decene	2,27 x10^{-12}	1,64 x10^{-11}	1,62 x10^{-11}
Nonene	1,51 x10^{-10}	9,37 x10^{-10}	9,27 x10^{-10}
Octane	5,58 x10^{-6}	2,43 x10^{-5}	2,37 x10^{-5}
Heptane	0,00012	0,00047	0,00046
Hexanal	3,37 x10^{-7}	1,75 x10^{-6}	1,74 x10^{-6}
Pentane	0,08251	0,23632	0,23182
Nonenal	8,25 x10^{-14}	9,16 x10^{-13}	9,18 x10^{-13}
Pentanal	6,11 x10^{-6}	2,66 x10^{-5}	2,64 x10^{-5}
Nonadiene	4,93 x10^{-15}	3,81 x10^{-14}	3,82 x10^{-14}
Methylhydroxyheptanoate	2,36 x10^{-13}	2,80 x10^{-12}	2,77 x10^{-12}
Methylhydroxy octanoate	6,92 x10^{-15}	1,13 x10^{-13}	1,12 x10^{-13}
Methyl-hydroxynonanoate	1,56 x10^{-14}	2,56 x10^{-13}	2,57 x10^{-13}
Methyl-8-oxooctanoate	5,20 x10^{-16}	9,59 x10^{-15}	1,13 x10^{-14}
Methyl heptanoate	1,08 x10^{-7}	6,46 x10^{-7}	6,42 x10^{-7}
Methyl octanoate	4,76 x10^{-10}	1,87 x10^{-9}	1,85 x10^{-9}
Methyl-9-oxononanoate	4,12 x10^{-16}	5,05 x10^{-15}	5,07 x10^{-15}
Methyl-8-oxooctanoate	4,59 x10^{-13}	5,70 x10^{-12}	5,73 x10^{-12}
Heptanal	1,83 x10^{-9}	1,15 x10^{-8}	1,14 x10^{-8}
Methyl-9-oxononanoate	1,56 x10^{-14}	2,56 x10^{-13}	2,57 x10^{-13}
Dimethyl octanedioate	6,82 x10^{-13}	8,55 x10^{-12}	8,60 x10^{-12}
Dimethyl nonanedioate	2,34 x10^{-14}	3,80 x10^{-13}	3,82 x10^{-13}
Ethanal	0,22335	0,53473	0,53586
Propanal	0,00668	0,01816	0,01812
Butanal	0,00017	0,00053	0,00053
Methylpyrrole	4,51 x10^{-13}	7,62 x10^{-13}	7,77 x10^{-13}
Pentadienal	2,27 x10^{-13}	1,19 x10^{-12}	1,23 x10^{-12}
Toluene	0,00024	0,00216	0,00224
Cycloheptadiene	0,02147	0,14142	0,14454